Products of the Benzene + O(^{3}P) Reaction

Craig A. Taatjes,[1,*] David L. Osborn,[1] Talitha M. Selby,[1†] Giovanni Meloni,[1‡] Adam J. Trevitt,[2§] Evgeny Epifanovsky,[3] Anna I. Krylov,[3] Baptiste Sirjean,[4] Enoch Dames,[4] Hai Wang[4,*]

1) Combustion Research Facility, Mailstop 9055, Sandia National Laboratories, Livermore, California, 94551-0969 USA

2) Departments of Chemistry and Physics, and Lawrence Berkeley National Laboratory, University of California, Berkeley, California, 94720 USA

3) Department of Chemistry, University of Southern California, Los Angeles, California, 90089-0482 USA

4) Department of Aerospace and Mechanical Engineering, University of Southern California, Los Angeles, California, 90089-1453 USA

* Corresponding author e-mail: cataatj@sandia.gov, haiw@usc.edu

Submitted to

Journal of Physical Chemistry A

December 1, 2009

Revised

January 2010

† Present address: Department of Chemistry, University of Wisconsin – Washington County, West Bend, WI 53095, USA

‡ Present address: Department of Chemistry, University of San Francisco, 2130 Fulton St., San Francisco, California 94117 USA

§ Present address: School of Chemistry, University of Wollongong, New South Wales 2522, Australia

ABSTRACT

The gas-phase reaction of benzene with $O(^3P)$ is of considerable interest for modeling of aromatic oxidation, and also because there exist fundamental questions concerning the prominence of intersystem crossing in the reaction. While its overall rate constant has been studied extensively, there are still significant uncertainties in the product distribution. The reaction proceeds mainly through the addition of the O atom to benzene, forming an initial triplet diradical adduct, which can either dissociate to form the phenoxy radical and H atom, or undergo intersystem crossing onto a singlet surface, followed by a multiplicity of internal isomerizations, leading to several possible reaction products. In this work, we examined the product branching ratios of the reaction between benzene and $O(^3P)$ over the temperature range of 300 to 1000 K and pressure range of 1 to 10 Torr. The reactions were initiated by pulsed-laser photolysis of NO_2 in the presence of benzene and helium buffer in a slow-flow reactor, and reaction products were identified by using the multiplexed chemical kinetics photoionization mass spectrometer operating at the Advanced Light Source (ALS) of Lawrence Berkeley National Laboratory. Phenol and phenoxy radical were detected and quantified. Cyclopentadiene and cyclopentadienyl radical were directly identified for the first time. Finally, ab initio calculations and master equation/RRKM modeling were used to reproduce the experimental branching ratios, yielding pressure-dependent rate expressions for the reaction channels, including phenoxy + H, phenol, cyclopentadiene + CO, which are proposed for kinetic modeling of benzene oxidation.

KEYWORDS: Gas-phase reaction kinetics, branching ratio, benzene, multiplexed photoionization mass spectrometer, ab initio methods, RRKM/master equation modeling

1. Introduction

Benzene is known to play a critical role in the combustion kinetics of hydrocarbon fuels,[1] and in the formation of both polycyclic aromatic hydrocarbons and soot from fuel-rich combustion.[2,3] Previously, a large number of chemical kinetic models have been proposed for benzene oxidation at high temperatures (see, for example, refs 4-12), yet the fundamental validity of these models as well as the models of other one-ring aromatics combustion is largely subject to uncertainties in the products and branching ratios of the reaction between benzene (C_6H_6, **1**) and the ground-state $O(^3P)$ atom

$$C_6H_6 + O(^3P) \rightarrow \text{products} . \quad \text{(R1)}$$

Extensive experimental studies[13-24] have led to some consensus on the total rate constant over the temperature range of 300 to 1400 K, as shown in Figure 1. Notably, Nicovich et al.[20] determined k_1 in argon over the temperature range of 298 to 950 K and at a pressure of 100 Torr. They proposed

$$k_1\left(\text{cm}^3\text{molecule}^{-1}\text{s}^{-1}\right) = 4.6\left(\pm 0.7\right)\times 10^{-11} e^{-(2470\pm 75)/T} \quad (1)$$

over the same temperature range. Leidreiter and Wagner[22] investigated the absolute rate constant of reaction R1 for temperature from 1200 to 1450 K and at a pressure of around 2 Torr in argon, and reported

$$k_1\left(\text{cm}^3\text{molecule}^{-1}\text{s}^{-1}\right) = 4.0\times 10^{-11} e^{-2350/T} . \quad (2)$$

Tappe et al.[23] made measurements for the absolute rate constant of R1 and reported

$$k_1\left(\text{cm}^3\text{molecule}^{-1}\text{s}^{-1}\right) = \left(3.5\pm 0.7\right)\times 10^{-11} e^{-(2250\pm 225)/T} . \quad (3)$$

for $305 \le T \le 865$ K and $270 \le P \le 850$ Torr (He). Ko et al.[24] determined k_1 over the temperature range of 600 to 1310 K and pressure from 180 to 450 Torr in argon. They reported a rate expression over that temperature range as

$$k_1\left(\mathrm{cm^3 molecule^{-1} s^{-1}}\right) = 5.4\times10^{-11} e^{-2610/T} \quad . \tag{4}$$

Experimental observations suggest that at or below a pressure of 1 bar, the total rate constant is essentially independent of pressure. based on these and other experimental observations, Baulch et al.[25] recommended a pressure-independent rate expression given as

$$k_1\left(\mathrm{cm^3 molecule^{-1} s^{-1}}\right) = 3.7\times10^{-11} e^{-2280/T} \quad , \tag{5}$$

for $298 \le T \le 1400$ K. The uncertainty in k_1 was estimated to be a factor of two.

CBS-QB3 calculations by Nguyen[26] showed that H abstraction by the O atom, leading to the phenyl and OH• radicals, has an energy barrier of around 12 kcal/mol, which is substantially larger than the measured activation energy at 4.5 kcal/mol. Hence, the H abstraction channel is expected to be unimportant; the measured reaction rates must be the result of O-atom addition to the benzene ring, followed by chemically activated processes, leading to the formation of several products. What remains uncertain is the product distribution. A multitude of exothermic reaction channels are possible, including[26]

$C_6H_6 + O(^3P) \rightarrow C_6H_5O\bullet$ (**3**) + H• (R1a)

$\rightarrow C_6H_5OH$ (**9**) (R1b)

$\rightarrow C_5H_6$ (**11**) + CO (R1c)

$\rightarrow$ isomers of C_6H_6OH.

In particular, the production of phenol (C_6H_5OH, **9**) or cyclopentadiene (C_5H_6, **11**) and CO leads to free-radical chain termination during benzene oxidation at high temperatures, whereas the production of the phenoxy radical (C_6H_5O•, **3**) and H atom provides secondary chain branching.

The reaction proceeds mainly through the addition of the O atom onto the ring to form a chemically activated triplet diradical (C_6H_6O**:**, **2**). Subsequent isomerization and decomposition of the diradical results in either C_6H_5O• + H• via a spin-conserved mechanism or it undergoes intersystem crossing onto singlet surfaces. Several experimental and theoretical studies have explored the fate of the initial triplet diradical and the products formed from reaction R1, as summarized in Table 1. Lee and co-workers[27] first detected the phenoxy radical in crossed molecular beams at a collision energy around 7 kcal/mol. Phenoxy as a reaction product was independently confirmed by Bajaj and Fontijn[28] in their flow reactor experiments at 450 K and between 3 to 12 Torr. While production of phenol is well established,[14,15,27-30] the production of cyclopentadiene and CO is controversial. Sloane[29] observed the formation of CO as a major product in his crossed molecular beam experiments at a collision energy of 0.6 kcal/mol. The production of CO is probably accompanied by cyclopentadiene formation, as in the case of phenol thermal decomposition.[31,32] On the other hand, Lee and co-workers[27] found CO to be a minor product in their crossed beam experiments at higher collision energies. Results of the flow reactor experiments of Nicovich et al.[20] and Bajaj and Fontijn[28] suggested that the yield of CO was less than 5% under their respective experimental conditions. Other isomers of phenol including benzene oxide, cyclohexadienone and butadienylketene, have also been detected as photolysis products of benzene/ozone mixtures in an argon matrix at 12 K by Parker and Davis.[33] In addition, Berndt and Bogo[30] reported the production of benzene oxide/oxepin in addition to phenol in the pressure range of 38 to 76 Torr and 297 K

Using the B3LYP density functional, Barckholtz et al.[34] examined the O(^{3}P) addition to benzene theoretically and found the calculated energy barrier (0.2 kcal/mol) to be substantially lower than the apparent activation energy measured experimentally (4-5 kcal/mol). Hodgson et al.[35] carried out CBS-QB3 and Rice-Ramsperger-Kassel-Marcus (RRKM) calculations for

reaction R1 on the triplet surface and suggested that the formation of phenoxy + H• and formylcyclopentadiene is dominant at low temperatures, while the decomposition of formylcyclopentadiene to form the cyclopentadienyl radical and HCO• is significant towards high temperatures. They also concluded that rearrangement of the C_6H_6O adduct to form phenol is unimportant at all temperatures. In a recent study, Nguyen et al.[26] concluded that the major products of reaction R1 include phenoxy + H atom, phenol and/or benzene oxide/oxepin, while cyclopentadiene + CO were predicted to be a minor channel, with a yield $\leq$ 5% under combustion conditions. They also noted that the initial O-addition to benzene can occur on two separate triplet surfaces, $^3A'$ and $^3A''$, and pointed out that Hodgson et al. were incorrect in characterizing the $^3A''$ triplet adduct as the lowest-energy state. Meanwhile, the complexity of the multiple spin states of the initial adduct ($^3A'$, $^3A''$, $^1A'$, $^1A''$) has been explored by Barckholtz et al.[36] using multi-reference CASSCF calculations.

Reaction R1 is characterized by processes on complex molecular potential energy surfaces, involving intersystem crossing, and competition between chemically activated bond dissociation and collisional stabilization of the adduct into multiple local minima on the singlet potential energy surface.[26,36] Furthermore, because of the large exothermicity associated with some of the reaction channels, dissociation of primary products may have to be taken into consideration. It is therefore not surprising that a wide range of conclusions have been reached experimentally with regard to dominant products and branching ratios. Although the total rate constant is insensitive to pressure variations, the product branching ratios are expected to strongly depend on temperature and pressure. Unfortunately, theoretical studies of this system have so far failed to provide conclusive guidance for the pressure and temperature dependence of the branching ratios for the various product channels observed. In particular, the inability of ab initio methods that can be afforded for this reaction has precluded accurate predictions for the reaction products, especially when intersystem crossing is one of the key processes.[36]

In the present work, we used a combination of experimental and theoretical approaches to determine the product branching ratios for reaction R1. We utilize the multiplexed chemical

kinetics photoionization mass spectrometer at the Advanced Light Source (ALS) of the Lawrence Berkeley National Laboratory to quantify the products of reaction R1 and their distribution over the temperature range of 300 to 1000 K and pressures from 1 to 10 Torr in helium. To facilitate data interpretation and extrapolation, we carried out high-level composite and multi-reference ab initio calculations to examine the initial triplet adducts and conducted master equation/RRKM modeling for the chemically activated processes following O atom addition to benzene.

2. Experiment

Experiments were performed at the Chemical Dynamics Beamline of the ALS using a side-sampled slow-flow reactor coupled to a multiplexed photoionization mass spectrometer. Neutral species, sampled from the flow reactor in real time, were ionized by continuously tunable vacuum ultraviolet synchrotron radiation with energies from 7.9 to 9.2 eV. The photoionization energy was limited in the present experiments by the ionization energy of benzene, because at higher photon energies the large benzene signal would saturate the detector. The experimental apparatus has been described previously and was used for both product identification and reaction kinetics studies.[37-39] Reactions are initiated in a slow flow quartz reactor by uniform pulsed-laser photolysis of NO_2 at 351 nm in helium, which generates $O(^3P)$ atoms.[40] The reacting mixture effuses from a pinhole located on the side of the reactor, passes through a skimmer, and enters the ionization region of a mass spectrometer, where the gas beam is crossed by tunable synchrotron radiation.

Most of the experiments reported here used a miniature double-focusing sector mass spectrometer;[38] however, higher mass-resolution experiments were also carried out with a new orthogonal-acceleration time-of-flight mass spectrometer[41] with pulsed extraction at 50 kHz. An entire time trace is collected for each photolysis pulse, giving a two-dimensional spectrum of the molecules emerging from the reactor as a function of their mass and the time relative to the photolysis. The photon energy of the synchrotron can be scanned during an acquisition yielding

a complete three-dimensional data set of time-resolved mass spectra as a function of photoionization energy.

Background subtraction was performed and the resulting signal was normalized at each photon energy against the ALS photon current and accumulated into the spectra. Figure 2 shows a typical example of the time-resolved integrated mass spectrum for the products of reaction R1 taken at 900K and 4 Torr. This spectrum was obtained using the miniature double-focusing magnetic-sector mass spectrometer, and represents an integration over photon energies between 7.9 and 9.1 eV. Figure 3 shows the corresponding photoionization efficiency spectrum (mass spectrum as a function of photon energy), where the integration of the three-dimensional data is now over reaction time, for the first 20 ms following the photolysis pulse.

Experiments were carried out for temperatures ranging from 300 to 1000 K and at pressures of 1, 4 and 10 Torr. The mass resolution of the perpendicular-extraction time-of-flight instrument is several thousand ($m/\Delta m$), that of the sector instrument less than about 150.[38] The phenoxy and phenol mass signals were only partially resolved in the sector experiments, and the radical product yields were therefore determined from the time-of-flight measurements.

The branching fractions were determined from the time-resolved mass spectrum taken at a photon energy of 9.1 eV, integrated over the first 20 ms following the photolysis pulse. As shown in Figure 2, the product concentrations rise rapidly following photolysis and remain nearly constant for at least 20 ms. Sections of the integrated mass spectrum are shown in Figure 4 for O + benzene at 900 K and 10 Torr. This time-integrated mass spectrum is further integrated over each mass peak, shown as the solid line in Figure 4, which gives the relative signal strength for each mass. The signals are then corrected for the photoionization cross section (see supporting material) and the empirically determined mass-dependent overall detection efficiency (approximately proportional to $(m/z)^{1/2}$ for the magnetic sector mass spectrometer detection and to (m/z) for the time-of-flight detection) to yield relative concentrations of phenol, phenoxy, cyclopentadiene and cyclopentadienyl. The reported

branching fractions to these four products are finally derived by imposing the condition that their sum is unity.

3. Computational Details

Electronic structure calculations. The potential energy surface of reaction (R1) is based on calculations reported previously[36] in which the multi-configurational CASSCF method was employed for the initial adducts. In this previous work, the active space was chosen to include 10 electrons in 9 orbitals. Orbitals considered in the active space were selected carefully and generally include: C-H σ and σ* orbitals of the H atom adjacent to the CO bond (2,2); the O lone pairs (3,2); and the π system (5,5). CASPT2 single points calculations were also performed including C-O σ and σ* orbitals. Critical geometries at conical intersections were investigated using methods proposed by Robb and co-workers and implemented in Gaussian 03.[42,43] To assess the results reported earlier, two sets of new calculations were performed here.

The molecular geometries and vibrational frequencies for all ground state closed-shell singlet and triplet stationary points were obtained from a modified version of G3B3[44] hereafter referred to as G3B3′. In this modified version of G3B3, geometries and vibrational frequencies were obtained at the B3LYP/6-311++G(d,p) level of theory (instead of B3LYP/6-31G(d) in the original G3B3 method) and the QCISD(T,E4T)/6-31G(d) step is replaced by a CCSD(T)/6-31G(d) single point calculation.

The four spin states of the initial adduct were investigated in detail using the equation-of-motion coupled-cluster (EOM-CC) approach which is capable of describing multiconfigurational systems within a single-reference formalism.[45] Geometry of the adduct was optimized at the EOM-EE-CCSD/6-311G(2d,p) level of theory in the $^3A'$ and $^3A''$ spin states using a high-energy closed-shell singlet reference state. Electronic states and vertical excitation energies were calculated for the $^3A'$ ground state with EOM-EE-CCSD/6-311G(2d,p) and EOM-DIP-CCSD/6-311G(2d,p). Both approaches employed closed-shell reference states, i.e., EOM-EE used a higher-energy closed-shell state, whereas the latter used the dianion reference.

Double-ionization potential (DIP) is a variant of the EOM approach where target states are found by detaching two electrons from the reference state,[46] whereas in EOM-EE particle and spin conserving operators are used. Conical intersection between $^3A'$ and the closed shell singlet state was computed using EOM-EE-CCSD. All electrons were frozen in EOM-CCSD calculations. G3B3′ calculations were performed with Gaussian 03 and EOM-CC calculations were performed with QChem.[47]

Adiabatic ionization energies. Ionization energies of many of the other possible C_6H_6O species on the PES of benzene + O(^{3}P) are unknown. For this reason, ab initio calculations were carried out to determine their values. Geometries, vibrational frequencies and energies of ground state singlet C_6H_6O isomers and their cations were determined by the CBS-QB3 method. Adiabatic ionization energies (IE) were calculated at 0 K with electronic energies including the standard scaled ZPE of the CBS-QB3 method. To achieve a better accuracy in the calculation of IEs, isodesmic reactions were also employed by following the procedure: (a) enthalpies of formation at 0 K of the parent ground-state singlet C_6H_6O isomer was determined using the average value of nine isodesmic reactions; (b) the enthalpy of formation at 0 K of the corresponding cation was established using the average value from three isodesmic reactions; (c) the "isodesmic" ionization energies were calculated with

$$IE\ (\text{CBS-QB3})_{\text{isodesmic}} = \Delta_f H^\circ_0(\text{cation}) - \Delta_f H^\circ_0\ (\text{neutral})\ . \qquad (6)$$

Reaction Rate Coefficients. Rate coefficients were calculated using an in-house Monte Carlo code for the solution of the master equation of collisional energy transfer.[48-50] Briefly, the time evolution of a rovibrationally excited molecule through the diradical adduct is described by the master equation in discrete form as

$$\frac{d[A(E_i)]}{dt} = \sum_j k_{ij}[M]\ [A(E_j)] - \sum_i k_{ji}[M]\ [A(E_i)] - \sum_m k_m(E_i)[A(E_i)] \qquad (7)$$

where $[A(E_i)]$ denotes the concentration of species A at the energy state E_i; $[M]$ is the third-body concentration; k_{ij} is the rate for the collision energy transfer from energy state j to i, and $k_m(E_i)$ is the microcanonical rate constant for the m^{th} channel, which also accounts for the dissociation of the adduct back to benzene + $O(^3P)$ and all reversible isomerizations. The microcanonical rate constants $k(E)$ are calculated using the conventional Rice-Ramsperger-Kassel-Markus (RRKM) expression. Details are given elsewhere.[51,52] The bimolecular rate coefficient of reaction R1 is determined by the equilibrium constant of C_6H_6 + $O(^3P)$ addition leading to the diradical adduct. The collisional energy transfer probability was described by the exponential down model, with $\langle E_{down} \rangle$ = 150 cm^{-1} for helium. As the scaling factor due to anharmonicity is well established for the B3LYP/6-311++G(d,p) vibrational frequencies (0.98),[53] partition functions are calculated using parameters obtained at this level of theory. Quantum tunneling was considered using the symmetric Eckart approach for reactions involving H-atom transfer.

4. Results and Discussion

Theoretical results. The potential energy surface obtained from quantum chemical calculations is presented on Figure 5. The global PES is very similar between the earlier CASSCF calculation[36] and current G3B3′ approach. The vertical energy gaps between different spin states of the initial adduct are summarized in Table 2. These gaps were obtained using several different multiconfigurational methods. At the CASSCF level of theory, the ground-state biradical adduct is characterized by the triplet $^3A'$ spin state, but the four states are found to be very close in energy (< 4 kcal/mol).[36] This result is in agreement with the CASSPT2(8,8)/cc-pVDZ//CASSCF(8,8)/cc-pVDZ results,[26] which showed that the four spin states lie in a range of 5.2 kcal/mol. EOM-CC calculations show a similar trend. Electronic states and vertical excitation energies calculated at the $^3A'$ equilibrium geometry show that the four spin states lie within 9.5 kcal/mol at the EOM-EE-CCSD/6-311G(2d,p) level of theory and 8.7 kcal/mol at the EOM-DIP-CCSD/6-311G(2d,p) level. In the DIP calculation, the reference is the closed-shell singlet state of the initial dianion adduct.

CASSCF and EOM-CC predict the same energy ordering of the spin states. The lowest energy spin state is $^3A'$ followed by $^1A'$, $^3A''$, and $^1A''$. The CASPT2-(8,8)/cc-pVDZ//CASSCF-(8,8)/cc-pVDZ results of Nguyen et al. show, however, a different ordering of the spin states.[26] In their calculations, the two triplet $^3A'$ and $^3A''$ states lie below the singlet states $^1A''$ and $^1A'$. As the CASSCF theory requires a selection of the active space that can be difficult, EOM-CC calculations presented here are expected to give a more accurate prediction of the ordering of the spin states. Regardless, all theoretical methods considered here show that there is a dense congregation of four electronic states within only a few kcal/mol from each other. A conical intersection was located between $^3A'$ and $^1A'$ states lying only 2.0 kcal/mol above the $^3A'$ minimum (blue line in Figure 5) suggesting that inter system crossing occurs easily, though more rigorous but expensive dynamic calculations are needed to provide a definitive conclusion.[36] This is beyond the scope of the present work.

Key geometric parameters obtained from EOM-EE-CCSD/6-311G(2d,p) geometry optimizations for $^3A'$ and $^3A''$ spin states of the initial adduct are presented on Figure 6. It is seen that the geometries of the $^3A'$ and $^3A''$ spin states are very close to each other. While bond lengths in the benzenoid rings are very close in the two spin states, the angle defined by the O atom, the tertiary carbon (C1) of the ring and the H atom bonded to C1 increases from $^3A'$ to $^3A''$. It is also worth noting that in the $^3A'$ state, the benzenoid ring is rather rigid with a deviation from planarity within 2°. However, for the $^3A''$ state the planarity of the ring is broken with a deviation from planarity around 7° and with C1 lifted towards O. Figure 7 shows frontier molecular orbitals for the initial adduct. The electronic configurations of the four spin states are as follows: $(n_{oop})^2(n_{ip})^1(\pi^*)^1$ for the triplet and singlet A′ states, $(n_{oop})^1(n_{ip})^2(\pi^*)^1$ for the $^3A''$ and $^1A''$states, with n_{oop} and n_{ip} being the respective out-of-plane and in-plane (relative to the molecular symmetry plane) oxygen lone pairs of a″ and a′ symmetries, and π* being the antibonding π MO of a′ symmetry. In the reference high-energy closed-shell singlet state all electrons are paired giving rise to a $^1A''/(n_{oop})^2(n_{ip})^2(\pi^*)^0$ occupation. Below these lone pairs lies an a″ molecular orbital corresponding to two C-C π-bonds on the ring (not shown). In the a″

orbital, there is an anti-bonding combination with sigma-bonding orbitals on C-C bonds adjacent to the oxygen. When a″ is occupied, the repulsion between the lone pair and the electron density of the ring increases. In the a′ orbital, there is an anti-bonding interaction between the lone pair and the sigma orbital on the C-H bond. When a′ is occupied, the O-H repulsion increases, leading to a larger O-C1-H angle. Therefore, in the state A′ stronger O-ring repulsion and weaker O/H repulsion leads to less C-O bond inclination towards the ring plane. In the A″ state, weaker O-ring repulsion and stronger O-H repulsion increases the O-C1-H angle and decreases the angle between the C-O bond and the ring plane. The geometries of diradical adducts in the ^{3}A′ and ^{3}A″ spin states obtained at the EOM-EE-CCSD/6-311G(2d,p) level of theory as well as vertical energy gaps at ^{3}A″ geometry may be found in the supplemental material.

As mentioned earlier, our CASSCF potential energy surface is very similar to that obtained from G3B3′. Table 3 lists the G3B3′ electronic energies and unscaled ZPEs for the stationary points of the PES presented in Figure 5, along with values derived from literature enthalpy of formation values.[54-59] With the exception of 2,4- and 2,5-cyclohexadienone, the computed and literature enthalpies of reaction are in reasonably good agreement. The enthalpy of formation values for 2,4- and 2,5-cyclohexadienone are reported by Shiner[57] to be $\Delta_f h^o_{298}$ = –17±3 and –13±3 kcal/mol, respectively. They are likely to be in error.[60] In general, previous theoretical results are in substantially better agreement with our ΔE(0K) values. For example, Recent CBS-QB3 results show that $\Delta_f h^o_{298}$ = –4.4 kcal/mol for 2,4-cyclohexadienone and –6.0 kcal/mol for 2,5-cyclohexadienone, which give ΔE(0K) = -83.1 and -84.7 kcal/mol, respectively, versus our values (–80.7 and –82.1 kcal/mol) as reported in Table 3.

At the G3B3' level of theory, the addition of O atom to the benzene ring occurs with a classical energy barrier of 5.7 kcal/mol. This value is in good agreement with the CBS-QB3 value of 4.9 kcal/mol reported by Nguyen et al.[26] and the experimental activation energy of 4-5 kcal/mol. The ^{3}A′ diradical adduct lies 11.4 kcal/mol below the energy of the entrance channel. This result is close to the CBS-QB3 value of 14.5 kcal/mol,[26] and confirms the erroneous attribution of the ^{3}A″ as the lowest-energy initial triplet adduct.[35]

Once formed, the rovibrationally excited diradical can undergo H-elimination to produce $C_6H_5O\bullet$ (**3**) + H• with a critical energy below that of reverse entrance channel, or it may undergo inter system crossing (ISC) onto the singlet surface following two separate mechanisms. The ISC can occur through a conical intersection between two spin states. This process is driven by dynamic effects on the PES and is complex for the reaction studied due to a dense congregation of four spin states leading to an interconnected PES. To better understand the ISC process in this system, the minimum-energy crossing point (MECP) between $^3A'$ and $^1A''$ closed-shell singlet states was investigated at the EOM-EE-CC/6-3111G(2d,p) level of theory using the method proposed by Epifanovsky and Krylov.[62] The MECP between these two spin states is only 1.4 kcal/mol above the $^3A'$ state, indicating that crossing into a singlet surface can occur with a rather small amount of energy. Geometry of the MECP is given in the supplemental information. Furthermore, starting from the ground-state triplet adduct, the first step of ISC can be a nonradiative transition to the singlet state of the adduct followed by isomerization to benzene oxide. CASSCF calculations showed that the isomerization process is almost barrierless. As the isomerization from the diradical adduct to benzene oxide is very exothermic (nearly 55 kcal/mol as predicted by CASSCF), each nonradiative transition should lead immediately to benzene oxide.

Once formed, benzene oxide can isomerize/dissociate to the various products detected experimentally. Routes to the most reported experimental products (see Table 1), cyclopentadiene(**11**) + CO and phenol (**9**), occur through the formation of 2,4-cyclohexadienone (**7**). The isomerization of benzene oxide to 2,4-cyclohexadienone (**5** → **7**) occurs with an energy barrier of 38.3 kcal/mol. 2,4-cyclohexadienone can isomerize to 2,5-cyclohexadienone (**8**), butadienyl ketene (**6**), phenol (**9**), or further decompose to cyclopentadiene + CO. The critical energies are estimated to be 51 and 60 kcal/mol for the formation of phenol and cyclopentadiene + CO from **7,** respectively. At high temperatures some of the cyclopentadiene product might undergo secondary dissociation to form the (overall endothermic) products CO + cyclopentadienyl + H atom, as shown in Figure 5.

It is also possible that the cyclopentadienyl radical can be produced directly through the formyl cyclopentadiene (C_5H_5CHO). Nguyen et al.[26] found that formyl cyclopentadiene may be produced from the initial $^3A'$ adduct on a triplet surface, but the energy barrier (~35 kcal/mol from the $^3A'$ adduct) is too high to be of any importance. Alternatively, formyl cyclopentadiene may be produced from benzene oxide on the singlet surface, but the energy barrier is 54 kcal/mol above benzene oxide, which is again too high to compete against other isomerization channels. In any case, Nguyen et al.[26] concluded that formyl cyclopentadiene dissociates primarily to cyclopentadiene + CO with an energy barrier around 27 kcal/mol, whereas the combined energies of cyclopentadienyl and HCO• lie ~40 kcal/mol higher than this energy barrier.

Experimental results. Product signals are observed at masses 94 (C_6H_6O), 93 (C_6H_5O), 66 (C_5H_6), and 65 (C_5H_5). According to previous experiments (Table 1) and to the potential energy surface presented in Figure 5, the signals at m/z = 93 and m/z = 65 can be identified as phenoxy radical and cyclopentadienyl. Photoionization efficiency (PIE) curves obtained at these masses show thresholds consistent with the reported ionization energies[63] of these two species (see supporting information). Moreover, although several C_6H_6O species are conceivable products of reaction 1, PIE curves allow the identification of phenol as the predominant species at m/z = 94. The photoionization efficiency curve of m/z = 94 at 700 K and above, presented in Figure 8 for 900 K, exhibits a gradual onset at around 8.5 eV, corresponding to the experimental ionization energy of phenol of 8.49 eV,[64] and is in excellent agreement with a calibration PIE spectrum of phenol, shown as the solid line.

At 300 and 500 K, small but significant signal was observed from one or more isomers with ionization energies near 8 eV (see supporting information). Because the IE for most of the C_6H_6O isomers are not known, we carried out CBS-QBS calculations for all isomers considered in the PES of Figure 5. Table 4 lists these IE values. Ionization energies obtained from isodesmic reactions are lower than that calculated directly with the CBS-QB3 theory, and are in good agreement with literature values. However, the IE calculated for benzene oxide is

substantially higher than that determined by Scagnolari et al.[65] from UV photoelectron spectroscopy. In their study, vertical ionization energies (VIE) were measured, but there are two issues worth considering. First, the photon electron spectrum of benzene oxide showed an unusually low intensity first band. Furthermore, benzene oxide can isomerize to oxepin with an almost negligible energy barrier (see, Figure 5). Scagnolari et al. assumed that benzene oxide is the single compound observed in the gas phase based on comparison with the spectrum of cycloheptatriene. We calculated the VIE of benzene oxide (**5**) and oxepin (**4**) using the CBS-QB3 method. Our results show that the VIE of benzene oxide is 9.16 eV and that of oxepin is 8.43 eV. Therefore we conclude that the reported VIE of benzene oxide may in fact be that of oxepin.

The ionization energies of oxepin and butadienyl ketene are below the minimum photon energy used in the present experiments. It is possible however that the small signals observed with ionization energy near 8 eV at 300 and 500 K are attributable to these isomers. At or above 700 K, however, the close agreement of the observed m/z = 94 PIE spectrum with that of phenol indicates that these isomers are minor contributors under these conditions.

The cyclohexadienone isomers have ionization energies near the upper limit of the photon energies in the present experiments (set by the need to remain below the 9.25 eV ionization energy of benzene). For this reason, their contributions cannot be ruled out. However, the master equation calculation suggests that branching into cyclohexadienones are rather insignificant.

The absolute cross section measurements of phenol and cyclopentadiene performed during this work (see supporting information) confirmed the identification of these two species and were used to quantify their relative concentrations. Cyclopentadiene and cyclopentadienyl radical are directly identified as products of the O + benzene reaction for the first time, although using crossed molecular beams in 1977, Sloane detected a mass signal at 66 he attributed (likely erroneously) to 3-penten-1-yne.[29] Time traces of phenol, phenoxy radical and cyclopentadiene / cyclopentadienyl radical (see Figure 2) all show a similar fast rise and a slow decay. These

profiles show that cyclopentadiene is only produced by the title reaction and that the contribution of thermal phenol decomposition to the production of C_5 species is negligible. This conclusion stands for all experimental conditions explored in this work.

Experimental branching ratios were determined as function of temperature for a constant pressure of 4 Torr, and as a function of pressure with temperature fixed at 800 K and 900 K. The branching ratios are found to be highly dependant on both pressure and temperature. Figure 9 presents experimental branching ratios as a function of temperature, ranging from 300 to 1000 K for a constant pressure of 4 Torr. As seen, at or below 500 K the dominant products are phenol and phenoxy + H. At 700 K, the production of phenol (R1b) decreases to slightly over one half of the distribution, whereas the production of cyclopentadiene (R1c) becomes significant. At 900 K, the ratios for the three dominant channels observed are about equal at 4 Torr.

Figure 10 presents the branching ratios observed at 800 K as a function of pressure, from 1 to 10 Torr. It is seen that phenol production rises with an increase in pressure, as expected due to enhanced collision stabilization. This is accompanied by the decrease in the rates of chemically activated dissociation to form cyclopentadiene + CO and phenoxy + H. The strong temperature and pressure dependencies observed here along with our theoretical calculations do explain some of the controversy over product distribution of the last 30 years, in that the different products and their dominance observed in these past studies are mostly likely the consequence of these dependencies.

We found the production of cyclopentadienyl radical to be small (less than 3%) over the entire ranges of temperature and pressure studied. As discussed before, the cyclopentadienyl radical can be produced from secondary dissociation of cyclopentadiene due to the exothermicity of reaction R1c. It can be formed also directly from isomerization of the initial triplet adducts followed by dissociation on the triplet surface.[35] We view the latter mechanism to be unlikely, considering that this triplet PES lies significantly higher than the singlet surface, and that the ISC is expected to be facile. Regardless, the weak signal measured from the cyclopentadienyl radical precludes the possibility to examine its production in greater detail.

The RRKM-master equation modeling by Nguyen et al.[26] predicted that the branching fractions are around 15, 3, and 75% for cyclopentadiene + CO, phenoxy + H, and phenol, respectively, at 700 K and 4 Torr. Their theoretical values are in fair agreement with the current measurements. These are, 22±5% for cyclopentadiene + CO, 18±8% for phenoxy + H, and 58±8% for phenol. Their theoretical prediction also includes the prediction of ~7% branching fraction for 2,4-cyclohexadienone at the same temperature and pressure. As we discussed earlier, the ionization energies of cyclohexadienone isomers are near the upper limit of the photon energies in the present experiments. Hence, no comparison can be made, though our theoretical results to be discussed below suggest the production of 2,4-cyclohexadienone to be somewhat lower than that predicted in Nguyen et al.[26]

Master equation modeling. Inter system crossing plays a crucial role in the product distribution and determining the ISC rate for the four dense spin states of the initial diradical adduct would require considerably demanding dynamic calculations. This is beyond the scope of the present study. In their theoretical work, Nguyen et al.[26] estimated the inter system crossing to be roughly 10^{11} s^{-1}. They concluded that dissociation of the adduct back to the reactants predominates above 1500 K while ISC dominates below 800 K. In between, the two routes are competitive. Here we used a semiempirical approach to determine the rate of inter system crossing. The method assumes that ISC can be described as a pseudo-saddle point; and its critical energy and geometry are equal to those of the critical point between the $^3A'$ diradical adduct and triplet benzene oxide from B3LYP density functional. The critical energy of this pseudo saddle point is then adjusted to reproduce experimental branching ratios, as the calculated phenol to phenoxy +H ratio (k_{1b}/k_{1a}) is very sensitive to this value. We chose a critical energy value for the pseudo-saddle point to be 11.3 kcal/mol above the $^3A'$ diradical adduct, which is close to the energy barrier calculated for H-elimination from the diradical adduct (12.7 kcal/mol).

To reproduce the experimental branching ratios, the critical energy for producing cyclopentadiene + CO from **10** (TS-**7**-**11**) was increased by 1.4 kcal/mol from the G3B3' value,

which is within the expected accuracy of the ab initio methods employed here. The energy barrier of the entrance channel was shifted upward by 0.4 kcal/mol to reproduce the total rate constant k_1 shown in Figure 1. Lastly, C-H fission in phenol, 2,4- and 2,5-cyclohexadienones to form phenoxy + H• are not considered in the modeling.

Because of its facile conversion to the much more stable 2,4-cyclohexadienone (**7**), butadienyl ketene (**6**) is expected to be a minor product (see Figure 5) and was not considered in the master equation modeling. Oxepin (**4**) was also not considered because it should rapidly reach equilibrium with benzene oxide, though neglecting it does cause the computation to under-estimate the density of state of the double well, thus over-estimating the microcanonical rate of benzene oxide isomerization to form 2,4-cyclohexadienone (**7**). Yet this treatment does affect the prediction of reaction products observed experimentally, as confirmed by a sensitivity calculation**.** Furthermore, isomer **10** was excluded from the calculation because it presents merely a shallow local minimum on the PES. The production of cyclopentadiene (**11**) + CO was assumed to proceed directly from 2,4-cyclohexadienone (**7**) through the critical geometry between **10** and **11** + CO, as shown in Figure 5. Processes considered in the master equations modeling were stabilization of rovibrationally excited complexes to form phenol (**9**), benzene oxide (**5**), 2,4-cyclohexadienone (**7**), 2,5-cyclohexadienone (**8**), and the dissociation into phenoxy (**3**) + H and cyclopentadiene (**11**) + CO, thus including six product channels: R1a-c and

$$C_6H_6 + O(^3P) \rightarrow \text{benzene oxide (}\mathbf{5}\text{)} \quad \text{(R1d)}$$

$$\rightarrow \text{2,4-cyclohexadienone (}\mathbf{7}\text{)} \quad \text{(R1e)}$$

$$\rightarrow \text{2,5-cyclohexadienone (}\mathbf{8}\text{).} \quad \text{(R1f)}$$

Table 5 presents the molecular parameters and the Lennard-Jones 12-6 potential parameters used for the RRKM/master equation modeling.

Reactions involving H-atom shift are inherently subject to effects of quantum tunneling. Within the framework of one-dimensional tunneling approximation, the large imaginary

frequency of TS-**7**-**9** (Table 5) suggests that tunneling can be important to this isomerization process. Therefore, temperature dependent transmission coefficients $\kappa(T)$ were calculated with the Eckart approach[68] using TheRate.[69] Transmission coefficients calculated at the G3B3' level of theory were implemented in RRKM/master equation simulations by lowering the critical energy of TS-**7**-**9** at a given temperature. Computational results show that quantum tunneling is critical to 2,4-cyclohexadienone isomerization to phenol, as $\kappa(T)$ is as large as 2.2×10^7 at 300 K. Such a considerable tunneling effect is equivalent to lowering the critical energy by 10.1 kcal/mol at that temperature. As temperature increases, transmission coefficients drop off rapidly with κ(400 K) = 225 and κ(500 K) = 2.3. Above 800 K, the tunneling effect becomes negligible as the transmission coefficient approaches unity. A rigorous treatment of the tunneling effect requires energy-specific corrections for each energy distribution of the chemically activated intermediates. This treatment was not attempted here. Since the primary purpose of the modeling work here is to extrapolate the experimental results, our tunneling treatment is sufficiently accurate.

RRKM/master equation modeling indicates that the total rate constant exhibits little to no pressure dependency, in agreement with the experiments. Figure 1 presents the rate constants computed at the high-pressure limit and in a 0.1 bar helium bath. The difference is negligible. The model predicts a minor curvature in the Arrhenius plot, whereas this curvature is not discernable experimentally. The curvature causes the predicted rate constant to be larger than the experimental rates by about 30% at 1400 K. Unfortunately very little experimental insights may be gained regarding this curvature. Not only are data unavailable at temperatures higher than 1400 K, experimental rates at such high temperatures can be complicated by benzene dissociation or isomerization. Theoretically, the curvature is caused by the low-frequency bending modes in the transition state of O atom addition to benzene. These modes are absent in benzene. Since there is no theoretical or experimental evidence to suggest that the low-frequency modes are grossly incorrect, the curvature is included in the rate expression we recommend here:

$$k_1\left(\mathrm{cm^3 molecule^{-1} s^{-1}}\right) = 1.6\times10^{-15} T^{1.4} e^{-1690/T} \quad (8)$$

for $300 \le T \le 2000$ K with an uncertainty factor of 2.

RRKM/master equation modeling satisfactorily reproduces the branching ratios observed over the entire experimental ranges of pressure and temperature, as seen in Table 6. In all cases, the computed branching ratios are well within the experimental uncertainties. In agreement with experiment, the computed yield of phenol (R1b) increases, while the branching fractions of phenoxy + H (R1a) and cyclopentadiene + CO (R1c) decrease somewhat from 4 to 10 Torr. Over the experimental conditions tested, reactions 1a-c account for over 90% of the total product yield. The sum of 2,4- and 2,5-cyclohexadienones and benzene oxide yields may be deduced from subtracting the values in the parentheses by the phenol or combined phenol and phenoxy yields (the last column of Table 6). It shows that for the experimental conditions tested, the production of 2,4- and 2,5-cyclohexadienones (**7** and **8**) is insignificant. The yield of 2,5-cyclohexadienone (**8**) is around 2% from 300 to 800 K, and decreases to < 1% at 1000 K. The same trend is observed for 2,4-cyclohexadienone (**7**) with an almost constant branching ratio of about 3% for temperatures < 800 K and around 1.5% at 1000 K. Likewise, benzene oxide can have yields around a few percent, representing the sum of benzene oxide and oxepin.

A small amount of benzene oxide and hexadienones are also computed at 300 and 500 K, as seen in Table 6. Since the IE for oxepin is around 7.7 eV (Table 4), it is possible that the small signal observed near 8 eV is due to oxepin, or conceivably to the neglected isomer butadienyl ketene. Additionally, with its IE equal to 8.9 eV, benzene oxide would have been observed experimentally but with the computed yield, its signal is probably too small to be discernable. The good agreement between master equation modeling and experimental branching fractions suggest that the pseudo-saddle point treatment for ISC is adequate. At 300 K, the high-pressure limit rate for ISC is 6000 s^{-1} compared to H-elimination at 2400 s^{-1} and back decomposition to C_6H_6 + O at 1 s^{-1}. At 1000 K, ISC is still the major path for the initial adduct with a frequency 3×10^{10} s^{-1}, compared to H elimination at 2.3×10^{10} s^{-1} and back

dissociation at 3×10^9 s^{-1}. These results show that ISC is facile for this system, as expected from the clustering of multiple spin states for the initial adducts with small energy splitting and similar molecular geometries.

Product yields were computed for reaction channels R1a-1f over the temperature range of 300 to 2000 K, and pressure from 0.1 to 500 bar. As seen in Figure 11, the yields show rather complex variations. Reaction channels R1a-c, leading to the formation of phenoxy, phenol, and cyclopentadiene, dominate under high-temperature and low-pressure conditions, whereas reaction channels R1d-1f, producing benzene oxide, 2,4- and 2,5-hexadienones are predominant at low temperatures and high pressures. With the exception of R1a (phenoxy + H•), rate constants of all other channels exhibit strong pressure dependency. This behavior is dictated by the competition among mutual isomerization of the C_6H_6O isomers, collisional stabilization of the isomers, and the dissociation of 2,4-cyclohexadienone. Excluded from Figure 11 is the initial adduct C_6H_6O ($^3A'$). Its production is found to be important at temperatures mostly below 700 K and high pressures (see Table S2 of the supplemental materials).

The computed yields are found to be in good agreement also with previous experimental results. For example, at 0.1 bar and up to 1000 K, the yield of CO through channel R1c is below 10%, which is in reasonable agreement with the Nicovich et al.'s observation of <5% CO production at 100 Torr.[20] Extrapolating the results of Figure 11 to 38-76 Torr, phenol and benzene oxide are indeed the dominant products at the room temperature, as observed by Berndt and Bogo.[30] Results presented earlier for pressures from 1 to 10 Torr indeed show phenol and phenoxy + H to be the main products at 400 K and the production of cyclopentadiene + CO to be minor at 405 K and 3-12 Torr. This is in agreement with the experimental results of Bajaj and Fontijn.[28]

5. Rate Constant Recommendations

The complex variations computed for the branching ratios of reaction R1 on pressure and temperature pose some challenges for kinetic modeling of benzene oxidation at high temperatures. Figure 12 presents the Monte Carlo RRKM/master equation modeling results of reaction channels R1a-f (symbols) and modified Arrhenius fits to the rate constants at 0.1, 1, 10, and 500 bar (lines). The modified Arrhenius parameters are also presented in Table 7. The computations were conducted with helium as the bath gas. At 1 bar pressure, for example, the branching ratios are

$$\frac{k_{1a}}{k_1}=0.23;\ \frac{k_{1b}}{k_1}=0.22;\ \frac{k_{1c}}{k_1}=0.02;\ \frac{k_{1d}}{k_1}=0.03;\ \frac{k_{1e}}{k_1}=0.31;\ \frac{k_{1f}}{k_1}=0.14 \text{ at 900 K,}$$

$$\frac{k_{1a}}{k_1}=0.29;\ \frac{k_{1b}}{k_1}=0.38;\ \frac{k_{1c}}{k_1}=0.10;\ \frac{k_{1d}}{k_1}=0.00;\ \frac{k_{1e}}{k_1}=0.09;\ \frac{k_{1f}}{k_1}=0.04 \text{ at 1300 K,}$$

$$\frac{k_{1a}}{k_1}=0.32;\ \frac{k_{1b}}{k_1}=0.37;\ \frac{k_{1c}}{k_1}=0.12;\ \frac{k_{1d}}{k_1}=0.00;\ \frac{k_{1e}}{k_1}=0.05;\ \frac{k_{1f}}{k_1}=0.03 \text{ at 1500 K.}$$

Clearly, the production of hexadienones (channels R1e and R1f) cannot be neglected. Towards higher pressures and, for example, at 10 bar, benzene oxide/oxepin should be considered,

$$\frac{k_{1a}}{k_1}=0.23;\ \frac{k_{1b}}{k_1}=0.03;\ \frac{k_{1c}}{k_1}=0.00;\ \frac{k_{1d}}{k_1}=0.28;\ \frac{k_{1e}}{k_1}=0.34;\ \frac{k_{1f}}{k_1}=0.07 \text{ at 900 K,}$$

$$\frac{k_{1a}}{k_1}=0.30;\ \frac{k_{1b}}{k_1}=0.20;\ \frac{k_{1c}}{k_1}=0.04;\ \frac{k_{1d}}{k_1}=0.02;\ \frac{k_{1e}}{k_1}=0.25;\ \frac{k_{1f}}{k_1}=0.11 \text{ at 1300 K,}$$

$$\frac{k_{1a}}{k_1}=0.32;\ \frac{k_{1b}}{k_1}=0.28;\ \frac{k_{1c}}{k_1}=0.06;\ \frac{k_{1d}}{k_1}=0.00;\ \frac{k_{1e}}{k_1}=0.05;\ \frac{k_{1f}}{k_1}=0.07 \text{ at 1500 K.}$$

Hence, a rigorous approach to simulate benzene oxidation must consider all six channels in a chemical kinetic model. On the other hand, inclusion of all six channels does add complexity

and additional uncertainties, since the reaction kinetics of benzene oxide, and 2,4- and 2,5-hexadienone are largely unknown.

An alternative approach is to consider these isomers of phenol to be in quasi-steady state upon production with phenol and cyclopentadiene + CO as the final products. With this assumption, the effective rate constants for production of phenol and cyclopentadiene + CO through these phenol isomers

$$C_6H_6 + O(^3P) \rightarrow [\mathbf{5},\mathbf{7},\mathbf{8}]_{ss} \rightarrow C_6H_5OH\ (\mathbf{9}) \qquad \text{(R1b-def)}$$

$$C_6H_6 + O(^3P) \rightarrow [\mathbf{5},\mathbf{7},\mathbf{8}]_{ss} \rightarrow C_5H_6\ (\mathbf{9}) + CO \qquad \text{(R1c-def)}$$

may be approximated by

$$k_{\text{1b-def}}^{\text{eff}}(T,P) = \frac{k_{\infty,\mathbf{7}\rightarrow\mathbf{9}}(T)}{k_{\infty,\mathbf{7}\rightarrow\mathbf{9}}(T) + k_{\infty,\mathbf{7}\rightarrow\mathbf{11}}(T)}\left[k_{\text{1d}}(T,P) + k_{\text{1e}}(T,P) + k_{\text{1f}}(T,P)\right] \qquad (9)$$

$$k_{\text{1c-def}}^{\text{eff}}(T,P) = \frac{k_{\infty,\mathbf{7}\rightarrow\mathbf{11}}(T)}{k_{\infty,\mathbf{7}\rightarrow\mathbf{9}}(T) + k_{\infty,\mathbf{7}\rightarrow\mathbf{11}}(T)}\left[k_{\text{1d}}(T,P) + k_{\text{1e}}(T,P) + k_{\text{1f}}(T,P)\right] \qquad (10)$$

where $k_{\infty,\mathbf{7}\rightarrow\mathbf{9}}$ and $k_{\infty,\mathbf{7}\rightarrow\mathbf{11}}$ are the high-pressure limit rate constants computed for 2,4-cyclohexadienone isomerization to phenol and dissociation to cyclopentadiene + CO, respectively. The rate constants $k_{\infty,\mathbf{7}\rightarrow\mathbf{9}}$ and $k_{\infty,\mathbf{7}\rightarrow\mathbf{11}}$ are computed here as

$$k_{\infty,\mathbf{7}\rightarrow\mathbf{9}}\left(\text{s}^{-1}\right) = 3.8\times10^{4}T^{2.38}e^{-22770/T}\ \ (500 \le T \le 2000\ \text{K}) \qquad (11)$$

and

$$k_{\infty,\mathbf{7}\rightarrow\mathbf{11}}\left(\text{s}^{-1}\right) = 1.5\times10^{12}T^{0.35}e^{-29860/T}\ \ (500 \le T \le 2000\ \text{K})\ . \qquad (12)$$

Table 7 shows the modified Arrhenius rate parameters fitted to $k_{\text{1b-def}}^{\text{eff}}$ and $k_{\text{1c-def}}^{\text{eff}}$ values from eqs 9 and 10 using the rate expressions given by eqs 11, 12, and those of k_{1d}, k_{1e}, and k_{1f} of the same table. In this alternative, semi-empirical approach, reaction R1 is simplified to three channels, leading to the production of phenoxy + H• (R1a), phenol (R1b), and cyclopentadiene + CO (R1c). The temperature- and pressure-dependent rate constant of phenol is approximated as the

sum of its intrinsic rate k_{1b} and the contributions from R1d-f ($k_{1b\text{-def}}^{\text{eff}}$); that of cyclopentadiene + CO is k_{1c} plus the contributions from R1d-f ($k_{1c\text{-def}}^{\text{eff}}$). At 1 bar pressure, for example, we have

R1a: $k_{1a}\left(\text{cm}^3\text{molecule}^{-1}\text{s}^{-1}\right) = 3.3\times10^{-17}T^{1.8}e^{-2000/T}$,

R1b: $k_{1b} + k_{1b\text{-def}}^{\text{eff}}\left(\text{cm}^3\text{molecule}^{-1}\text{s}^{-1}\right) = 1.2\times10^{-1}T^{-2.56}e^{-7546/T} + 2.5\times10^{-3}T^{-2.60}e^{-3364/T}$,

R1c: $k_{1c} + k_{1c\text{-def}}^{\text{eff}}\left(\text{cm}^3\text{molecule}^{-1}\text{s}^{-1}\right) = 1.0\times10^{-8}T^{-0.49}e^{-7546/T} + 1.2\times10^{5}T^{-4.66}e^{-10469/T}$

with an applicable temperature range of 500 – 2000 K. These expressions are derived from calculations with helium as the bath gas. For nitrogen and argon, the rates of collision stabilization channels R1b is expected to be somewhat larger than what is presented above and the dissociation channels are correspondingly slower. Considering the uncertainty of the total rate constant to be a factor of 2, the use of rate expressions derived from these calculations should be sufficiently accurate.

6. Conclusion

The branching ratios of the gas-phase reaction between benzene and O(^{3}P) atom were investigated experimentally by pulsed-laser photolysis of NO_2 in a flow reactor over the temperature range of 300 to 1000 K and pressures from 1 to 10 Torr. The products were identified and quantified using the multiplexed chemical kinetics photoionization mass spectrometer. Under the experimental conditions studied, the dominant products observed include phenol, phenoxy and cyclopentadiene; their yields strongly depend on pressure and temperature. At or below 500 K, the dominant product is phenol, along with some phenoxy + H. Above 700 K, the production of phenoxy + H and cyclopentadiene + CO was observed to be significant.

The potential energy of the reaction was examined using several multi- and single-reference methods with specific emphasis placed on different spin states of the initial adduct of

O atom addition to benzene. Results confirm the clustering of multiple spin states with small energy gaps for the initial adduct and suggest that the intersystem crossing is likely to be facile. RRKM/Master equation modeling was carried out to extrapolate the experimentally measured branching ratios to wide ranges of pressure and temperature. Treating the intersystem crossing as a pseudo-saddle point on the potential energy surfaces, we showed that upon appropriate adjustments made to several PES parameters the computed branching ratios are in close agreement with the experimental data over the entire ranges of pressure and temperature considered. In addition, the total rate constant was computed to be nearly independent of pressure, in agreement with a large number of rate measurements reported in the literature. Based on the experimental branching ratios and comparisons made between model and experiment, pressure-dependent rate expressions are proposed for reaction R1 over the temperature and pressure ranges of interest to combustion modeling.

7. Acknowledgements

This work is supported by the Division of Chemical Sciences, Geosciences, and Biosciences, the Office of Basic Energy Sciences, the U. S. Department of Energy Sandia is a multi-program laboratory operated by Sandia Corporation, a Lockheed Martin Company, for the National Nuclear Security Administration under contract DE-AC04-94-AL85000. The Advanced Light Source is supported by the Director, Office of Science, Office of Basic Energy Sciences, Materials Sciences Division, of the U.S. Department of Energy under Contract No. DE-AC02-05CH11231 at Lawrence Berkeley National Laboratory. The support of personnel (A.J.T.) for this research by the National Aeronautics and Space Administration (grant NAGS-13339) is gratefully acknowledged. BS, ED and HW acknowledge support for the part of the work concerning master equation modeling by the Combustion Energy Frontier Research Center (CEFRC), an Energy Frontier Research Center funded by the U.S. Department of Energy, Office of Science, Office of Basic Energy Sciences under Award Number DE-SC0001198. The support

of personnel (A.J.T.) for this research by the National Aeronautics and Space Administration (grant NAGS-13339) is gratefully acknowledged. HW also acknowledges partial support by the Air Force of Scientific Research (Grant No. FA9550-07-1-0168) and by the Strategic Environmental Research and Developmental Program (SERDP). AIK and EE acknowledge support of the Department of Energy (DE-FG02-05ER1-5685).

8. Supporting Information Available: Photoionization cross section measurements, geometries of EOM-EE-CC calculations, and Monte Carlo results of product yield as functions of temperature (300 to 2000 K) and pressure (0.1 to 500 bar). This material is available free of charge via the Internet at http://pubs.acs.org.

9. References

(1) Glassman, I. *Combustion 2nd Ed.*; Academic press: Boca Raton, FL, 1987.
(2) Frenklach, M.; Wang, H. *Symp. (Int.) Combust.* **1991**, *23*, 1559.
(3) Wang, H.; Frenklach, M. *Combust. Flame* **1997**, *110*, 173.
(4) Emdee, J. L.; Brezinsky, K.; Glassman, I. *J. Phys. Chem.* **1992**, *96*, 2151.
(5) Zhang, H. Y.; McKinnon, J. T. *Combust. Sci. Technol.* **1995**, *107*, 261.
(6) Davis, S. G.; Wang, H.; Brezinsky, K.; Law, C. K. *Symp. (Int.) Combust.* **1996**, *26*, 1025.
(7) Alzueta, M. U.; Glarborg, P.; Dam-Johansen, K. *Int. J. Chem. Kinet.* **2000**, *32*, 498.
(8) Ristori, A.; Dagaut, P.; El Bakali, A.; Pengloan, G.; Cathonnet, M. *Combust. Sci. Technol.* **2001**, *167*, 223.
(9) Richter, H.; Howard, J. B. *Phys. Chem. Chem. Phys.* **2002**, *4*, 2038.
(10) Da Costa, I.; Fournet, R.; Billaud, F.; Battin-Leclerc, F. *Int. J. Chem. Kinet.* **2003**, *35*, 503.
(11) Richter, H.; Granata, S.; Green, W. H.; Howard, J. B. *Proc. Combust. Inst.* **2005**, *30*, 1397.
(12) Detilleux, V.; Vandooren, J. *Combust. Explosion Shock Wave.* **2009**, *45*, 392.
(13) Boocock, G.; Cvetanovic, R. J. *Can. J. Chem.* **1961**, *39*, 2436.
(14) Mani, I.; M.C. Sauer, J. *Adv. Chem. Ser.* **1968**, *82*, 142.
(15) Bonanno, R. A.; Timmons, R. B.; Lee, J. H.; Kim, P. *J. Chem. Phys.* **1972**, *57*, 1377.
(16) Atkinson, R.; Pitts, J. N. *J. Phys. Chem.* **1974**, *78*, 1780.
(17) Atkinson, R.; Pitts, J. N. *J. Phys. Chem.* **1975**, *79*, 295.
(18) Colussi, A. J.; Singleton, D. L.; Irwin, R. S.; Cvetanovic, R. J. *J. Phys. Chem.* **1975**, *79*, 1900.
(19) Atkinson, R.; Pitts, J. N. *Chem. Phys. Lett.* **1979**, *63*, 485.
(20) Nicovich, J. M.; Gump, C. A.; Ravishankara, A. R. *J. Phys. Chem.* **1982**, *86*, 1684.
(21) Tabares, F. L.; Urena, A. G. *J. Phys. Chem.* **1983**, *87*, 4933.
(22) Leidreiter, H. I.; Wagner, H. G. *Z. Phys. Chem. (Neue Folge)* **1989**, *165*.
(23) Tappe, M.; Schliephake, V.; Wagner, H. G. *Z. Phys. Chem. (Neue Folge)* **1989**, *162*, 129.
(24) Ko, T.; Adusei, G. Y.; Fontijn, A. *J. Phys. Chem.* **1991**, *95*, 8745.
(25) Baulch, D. L.; Bowman, C. T.; Cobos, C. J.; Cox, R. A.; Just, T.; Kerr, J. A.; Pilling, M. J.; Stocker, D.; Troe, J.; Tsang, W.; Walker, R. W.; Warnatz, J. *J. Phys. Chem. Ref. Data* **2005**, *34*, 757.
(26) Nguyen, T. L.; Peeters, J.; Vereecken, L. *J. Phys. Chem. A* **2007**, *111*, 3836.
(27) Sibener, S. J.; Buss, R. J.; Casavecchia, P.; Hirooka, T.; Lee, Y. T. *J. Chem. Phys.* **1980**, *72*, 4341.
(28) Bajaj, P. N.; Fontijn, A. *Combust. Flame* **1996**, *105*, 239.
(29) Sloane, T. M. *J. Chem. Phys.* **1977**, *67*, 2267.
(30) Berndt, T.; Boge, O. *Z. Phys. Chemie-Int. J. Res. Phys. Chem. Chem. Phys.* **2004**, *218*, 391.
(31) Horn, C.; Roy, K.; Frank, P.; Just, T. *Symp. (Int.) Combust.* **1998**, *27*, 321.
(32) Xu, Z. F.; Lin, M. C. *J. Phys. Chem. A* **2006**, *110*, 1672.

(33) Parker, J. K.; Davis, S. R. *J. Am. Chem. Soc.* **1999**, *121*, 4271.
(34) Barckholtz, C.; Barckholtz, T. A.; Hadad, C. M. *J. Phys. Chem. A* **2001**, *105*, 140.
(35) Hodgson, D.; Zhang, H. Y.; Nimlos, M. R.; McKinnon, J. T. *J. Phys. Chem. A* **2001**, *105*, 4316.
(36) Barckholtz, T. A.; Joshi, A.; Wang, H. In *4th Joint Meeting of the U.S. Sections of the Combustion Institute* Drexel University, Philadelphia, Pennsylvania, 2005.
(37) Taatjes, C. A.; Hansen, N.; Osborn, D. L.; Kohse-Hoinghaus, K.; Cool, T. A.; Westmoreland, P. R. *Phys. Chem. Chem. Phys.* **2008**, *10*, 20.
(38) Osborn, D. L.; Zou, P.; Johnsen, H.; Hayden, C. C.; Taatjes, C. A.; Knyazev, V. D.; North, S. W.; Peterka, D. S.; Ahmed, M.; Leone, S. R. *Rev. Sci. Instrum.* **2008**, *79*, 104103.
(39) Selby, T. M.; Meloni, G.; Goulay, F.; Leone, S. R.; Fahr, A.; Taatjes, C.; Osborn, D. L. *J. Phys. Chem. A* **2008**, *112*, 9366.
(40) Pitts Jr., J. N.; Sharp, J. H.; Chan, S. I. *J. Chem. Phys.* **1964**, *42*, 3655.
(41) Coles, J.; Guilhaus, M. *Trac-Trend Anal. Chem.* **1993**, *12*, 203.
(42) Garcia-Exposito, E.; Bearpark, M. J.; Ortuno, R. M.; Branchadell, V.; Robb, M. A.; Wilsey, S. *J. Org. Chem.* **2001**, *66*, 8811.
(43) Frisch, M. J. e. a. *Gaussian 03, Revision C.02, Gaussian Inc, Wallingford, CT 2004.*
(44) Baboul, A. G.; Curtiss, L. A.; Redfern, P. C.; Raghavachari, K. *J. Chem. Phys.* **1999**, *110*, 7650.
(45) Krylov, A. I. *Annu. Rev. Phys. Chem.* **2008**, *59*, 433.
(46) Wladyslawski, M.; Nooijen, M. *ACS Symp. Ser.* **2002**, *828*, 65.
(47) Shao, Y.; Molnar, L. F.; Jung, Y.; Kussmann, J.; Ochsenfeld, C.; Brown, S. T.; Gilbert, A. T. B.; Slipchenko, L. V.; Levchenko, S. V.; O'Neill, D. P.; DiStasio, R. A.; Lochan, R. C.; Wang, T.; Beran, G. J. O.; Besley, N. A.; Herbert, J. M.; Lin, C. Y.; Van Voorhis, T.; Chien, S. H.; Sodt, A.; Steele, R. P.; Rassolov, V. A.; Maslen, P. E.; Korambath, P. P.; Adamson, R. D.; Austin, B.; Baker, J.; Byrd, E. F. C.; Dachsel, H.; Doerksen, R. J.; Dreuw, A.; Dunietz, B. D.; Dutoi, A. D.; Furlani, T. R.; Gwaltney, S. R.; Heyden, A.; Hirata, S.; Hsu, C. P.; Kedziora, G.; Khalliulin, R. Z.; Klunzinger, P.; Lee, A. M.; Lee, M. S.; Liang, W.; Lotan, I.; Nair, N.; Peters, B.; Proynov, E. I.; Pieniazek, P. A.; Rhee, Y. M.; Ritchie, J.; Rosta, E.; Sherrill, C. D.; Simmonett, A. C.; Subotnik, J. E.; Woodcock, H. L.; Zhang, W.; Bell, A. T.; Chakraborty, A. K.; Chipman, D. M.; Keil, F. J.; Warshel, A.; Hehre, W. J.; Schaefer, H. F.; Kong, J.; Krylov, A. I.; Gill, P. M. W.; Head-Gordon, M. *Phys. Chem. Chem. Phys.* **2006**, *8*, 3172.
(48) Joshi, A. V.; Wang, H. *Int. J. Chem. Kinet.* **2006**, *38*, 57.
(49) Joshi, A.; You, X. Q.; Barckholtz, T. A.; Wang, H. *J. Phys. Chem. A* **2005**, *109*, 8016.
(50) You, X. Q.; Wang, H.; Goos, E.; Sung, C. J.; Klippenstein, S. J. *J. Phys. Chem. A* **2007**, *111*, 4031.
(51) Wang, H.; Frenklach, M. *J. Phys. Chem.* **1994**, *98*, 11465.
(52) Davis, S. G.; Law, C. K.; Wang, H. *J. Phys. Chem. A* **1999**, *103*, 5889.
(53) Andersson, M. P.; Uvdal, P. *J. Phys. Chem. A* **2005**, *109*, 2937.
(54) Roux, M. V.; Temprado, M.; Chickos, J. S.; Nagano, Y. *J. Phys. Chem. Ref. Data* **2008**, *37*, 1855.
(55) Cox, J. D.; Wagman, D. D.; Medvedev, V. A. *CODATA Key Values for Thermodynamics*; Hemisphere Publishing Corp.: New York, 1984.

(56) Tsang, W. Heats of Formation of Organic Free Radicals by Kinetic Methods. In *Energetics of Organic Free Radicals*; Martinho Simoes, J. A. G., A., Liebman, J. F., Eds.; Blackie Academic and Professional: London, 1996; pp 22.

(57) Shiner, C. S.; Vorndam, P. E.; Kass, S. R. *J. Am. Chem. Soc.* **1986**, *108*, 5699.

(58) Cox, J. D. *Pure Appl. Chem.* **1961**, *2*, 125.

(59) Roth, W. R.; Adamczak, O.; Breuckmann, R.; Lennartz, H.-W.; Boese, R. *Chem. Ber.* **1991**, *124*, 2499.

(60) Zhu, L.; Bozzelli, J. W. *J. Phys. Chem. A* **2003**, *107*, 3696.

(61) Santoro, D.; Louw, R. *J. Chem. Soc., Perkin Trans. 2* **2001**, *4*, 645.

(62) Epifanovsky, E.; Krylov, A. I. *Molecular Physics* **2007**, *105*, 2515.

(63) Lias, S. G.; Bartmess, J. E.; Liebman, J. F.; Holmes, J. L.; Levin, R. D.; Mallard, W. G. Ion Energetics Data. In *NIST Chemistry WebBook, NIST Standard Reference Database Number 69*; Linstrom, P. J., Mallard, W. G., Eds.; National Institute of Standards and Technology: Gaithersburg, MD, 2003.

(64) Lias, S. G. Ionization Energy Evaluation. In *NIST Chemistry WebBook, NIST Standard Reference Database Number 69*; Linstrom, P. J., Mallard, W. G., Eds.; National Institute of Standards and Technology: Gaithersburg, MD, 20899, 2005.

(65) Scagnolari, F.; Modelli, A.; Bottoni, A.; Jones, D.; Lazzari, D. *J. Chem. Soc.-Faraday Trans.* **1996**, *92*, 1447.

(66) Le, H. T.; Flammang, R.; Gerbaux, P.; Bouchoux, G.; Nguyen, M. T. *J. Phys. Chem. A* **2001**, *105*, 11582.

(67) Yang, B.; Li, Y.; Wei, L.; Huang, C.; Wang, J.; Tian, Z.; Yang, R.; Sheng, L.; Zhang, Y.; Qi, F. *Proc. Combust. Inst.* **2007**, *31*, 555.

(68) Eckart, C. *Phys. Rev.* **1930**, *35*, 1303.

(69) Duncan, W. T.; Bell, R. L.; Truong, T. N. *J. Comp. Chem.* **1998**, *19*, 1039.

Table 1. Summary of literature studies on the products observed for reaction (R1)

Reference	Experiment type	Conditions	Products
Sloane[29]	Crossed molecular beams	Collision energy = 0.6 kcal/mol	phenol CO (major)
Sibener et al.[27]	Crossed molecular beams	Collision energies = 6.5 / 8.5 kcal/mol	phenoxy + H phenol CO ≤ 5%
Nicovich et al.[20]	Flow reactor	298-950 K, 100 Torr	CO ≤ 5%
Bajaj and Fontijn[28]	Flow reactor	405 K, 3-12 Torr	phenoxy + H phenol CO minor (≤ 5%)
Parker and Davis[33]	Photolysis of benzene/ ozone mixtures in argon matrix	12 K	benzene oxide cyclohexadienone butadienylketene
Berndt and Bogo[30]	Flow reactor	295 K, 38-76 Torr	phenol, benzene oxide/oxepin

Table 2. Calculated energy gaps (kcal/mol) among the four spin states (^{3}A′, ^{3}A″, ^{1}A′, ^{1}A″) of the initial adduct of reaction R1.

	CASSCF(10,9)/ 6-31G(d)[a,b]	CASPT2(8,8)/cc-pVDZ// UB3LYP/6-311G(d,p)[a,c]	EOM-EE-CCSD /6-311G(2d,p)[d]	EOM-DIP-CCSD /6-311G(2d,p)[d]
^{3}A′	0.0	0.0	0.0	0.0
^{1}A′	1.7	5.2	4.7	2.7
^{3}A″	3.0	2.7	6.1	6.9
^{1}A″	3.1	5.1	9.5	8.7

[a] Adiabatic energy gap, including zero-point energy. [b] Taken from Barckholtz et al.[36] [c] Taken from Nguyen et al.[26] [d] Vertical energy gaps at the ^{3}A′ geometry (this work).

Table 3. Electronic energies E_0 (Hartree), zero point energies (ZPE, Hartree) and relative energies at 0 K (kcal/mol) for species involved in reaction R1 determined at the G3B3′ level of theory (see text). Also included are the available literature values.

			ΔE (0K)	
Species	E_0	ZPE	calc[a]	Literature[b]
Benzene (**1**) + O(^{3}P)	–306.66755	0.10009	0.0	0.0
Initial adduct C_6H_6O (^{3}A′, **1**)	–306.68490	0.09931	–11.4	
Phenoxy (**3**) + H	–306.67799	0.09096	–12.3	-14.6±1.0[c]
Oxepin (**4**)	–306.75778	0.10271	–55.0	
Benzene oxide (**5**)	–306.75850	0.10354	–54.9	
Butadienyl ketene (**6**)	–306.74986	0.09958	–52.0	
2,4-cyclohexadienone (**7**)	–306.79891	0.10277	–80.7	–95.7±3.0[d]
2,5-cyclohexadienone (**8**)	–306.80135	0.10311	–82.1	–91.7±3.0[d]
Phenol (**9**)	–306.82683	0.10394	–97.5	–101.7±0.2[e]
Bicyclo[3.1.0]hex-2-en-6-one (**10**)	–306.74864	0.10196	–49.7	
Cyclopentadiene (**11**) + CO	–306.78002	0.09714	–72.4	–73.0[f]
TS **1**–**2** (^{3}A′ state)	–306.65817	0.09978	5.7	
TS **2**–**3**	–306.65866	0.09334	1.3	
TS **4**–**5**	–306.74608	0.10187	–48.2	
TS **5**–**7**	–306.69293	0.09904	–16.6	
TS **6**–**7**	–306.73515	0.09957	–42.7	
TS **7**–**8**	–306.72357	0.09881	–36.0	
TS **7**–**9**	–306.71210	0.09744	–29.6	
TS **7**–**10**	–306.72293	0.09883	–35.5	
TS **10**–**11**	–306.69986	0.09926	–20.8	

[a] This work. [b] Relative to benzene ($\Delta_f h^o_{298}$ = 19.8±0.2 kcal/mol[54]) and O atom ($\Delta_f h^o_{298}$ = 59.6 kcal/mol[55]). Values of the enthalpy of reaction were calculated from standard enthalpy of formation at 298 K, converted to 0 K though sensible enthalpies. [c] $\Delta_f h^o_{298}$ (C_6H_5O) = 13±1 kcal/mol.[56] and $\Delta_f h^o_{298}$ (H) = 52.1 kcal/mol.[55] [d] Derived from Shiner et al.[57] They are the most likely to be in error (see text). [e] Calculated from $\Delta_f h^o_{298}$ (C_6H_5OH) = –23.0±0.6 kcal/mol.[58] [f] Based on $\Delta_f h^o_{298}$ (C_5H_6) = 33.2[59] and $\Delta_f h^o_{298}$ (CO) = –26.4 kcal/mol.[55]

Table 4. Adiabatic ionization energies (eV) of the C_6H_6O isomers.

Species	CBS-QB3	Isodesmic	Literature
Oxepin (**4**)	7.77	7.72	
Benzene oxide (**5**)	8.90	8.85	8.43 ± 0.05[65]
Butadienyl ketene (**6**)	7.94	7.89	
2,4-cyclohexadienone (**7**)	9.05	9.01	9.11[a]
2,5-cyclohexadienone (**8**)	9.30	9.25	9.3 [a]
Phenol (**9**)	8.56	8.52	8.48 ± 0.02[67]

[a] Evaluated using DFT calculations of Le et al.[66]

Table 5. Molecular parameters used in RRKM/master equation modeling.

Stable species/ critical geometry	E_0[a] (kcal/mol)	B (cm^{-1}) Active[b]	Inactive[c]	Vibrational frequency, v (cm^{-1})																
C_6H_6O ($^3A'$, **1**)	–11.4	0.166	0.076	114	302	411	421	525	576	611	704	735	799	843	933	962	967	989	1013	1049
				1077	1134	1157	1197	1222	1331	1383	1440	1534	1589	2686	3159	3162				
Benzene oxide (**5**)	–54.9	0.153	0.095	253	315	461	543	615	630	696	769	776	841	935	974	977	980	988	1008	1058
				1135	1189	1204	1255	1363	1377	1423	1461	1596	1679	3122	3130	3159	3168	3180	3188	
2,4-cyclohexadie-none (**7**)	–82.0	0.173	0.073	53	269	443	457	495	538	580	723	745	811	941	946	955	997	998	1021	1162
				1193	1195	1247	1336	1398	1406	1444	1604	1687	1727	3015	3034	3154	3159	3184	3191	
2,5-cyclohexadie-none (**8**)	–80.7	0.175	0.073	122	312	361	457	507	574	578	749	771	851	882	943	964	992	1011	1025	1143
				1194	1205	1273	1376	1415	1416	1427	1652	1687	1725	2989	2997	3149	3149	3183	3185	
C_6H_5OH (**9**)	–97.5	0.189	0.072	228	312	405	417	509	536	633	669	749	819	827	878	952	972	1013	1043	1093
				1176	1190	1191	1275	1348	1368	1499	1527	1635	1646	3149	3167	3176	3190	3197	3836	
TS-**1**-**2** ($^3A'$ state)	6.2	0.146	0.076	412*i*	106	132	391	402	604	612	658	726	820	896	930	975	991	1007	1027	1037
				1049	1169	1173	1195	1331	1368	1470	1480	1573	1604	3140	3167	3178	3189	3195	3200	
TS-**2**-**3**	1.3	0.176	0.074	1009*i*	166	358	429	482	512	552	594	643	704	764	792	842	914	977	978	980
				1004	1087	1159	1167	1265	1332	1338	1429	1455	1538	1584	3166	3171	3190	3197	3200	
TS-**2**-**5** (ISC)[d]	1.1	0.154	0.091	541*i*	178	305	379	437	545	578	628	673	760	817	880	941	948	966	981	1032
				1074	1150	1185	1231	1350	1384	1404	1419	1454	1587	3061	3167	3182	3187	3198	3213	
TS-**5**-**7**	–16.6	0.165	0.078	763*i*	233	265	420	509	569	580	717	750	782	931	956	988	1001	1017	1021	1060
				1111	1150	1182	1197	1295	1373	1422	1454	1542	1608	2423	3160	3173	3182	3191	3215	
TS-**7**-**8**	–36.0	0.183	0.072	837*i*	132	382	432	451	518	591	643	707	801	806	868	942	978	994	1002	1054
				1153	1173	1229	1266	1337	1400	1431	1529	1547	1649	2472	3144	3159	3182	3194	3213	
TS-**7**-**9**[e]	–29.6	0.175	0.077	2138*i*	214	360	458	519	525	613	632	751	773	829	869	958	987	998	1003	1074
				1116	1172	1181	1263	1369	1390	1453	1512	1538	1618	1790	3084	3161	3171	3193	3198	
TS-**7**-**11**	–20.8	0.163	0.081	622*i*	121	222	291	441	510	536	663	727	796	847	914	936	947	1005	1021	1050
				1112	1145	1205	1241	1287	1303	1387	1477	1531	2024	2941	3103	3112	3188	3224	3260	

Species	$\langle E_{down} \rangle$ (cm^{-1})	σ (Å)	ε/k_B (K)
He	150	2.58	10.2
Adduct (C_6H_6O)		5.29	465

K_{eq} (cm^3mol^{-1}) = $3.23\times10^{-06}\ T^{1.71}\ e^{15060/T}$ for $C_6H_6 + O(^3P) \rightarrow C_6H_6O\ (^3A')$

[a] Energy relative to that of the entrance channel. [b] Two-dimensional (all symmetry number σ =1); [c] One-dimensional (all symmetry number σ =1). [d] Pseudo critical geometry (see text). [e] With Eckart tunneling (see text).

Table 6. Branching ratios experimentally determined and computed for reaction R1.

			Branching ratio	
Reaction channel	*P* (Torr)	*T* (K)	Experimental	Computational
C_6H_5OH (**9**)	4	700	0.58 ± 0.08[a]	0.56 (0.65)[d]
	4	800	0.47 ± 0.08[a]	0.43 (0.50)[d]
	4	900	0.33 ± 0.08[a]	0.29 (0.37)[d]
	10	800	0.59 ± 0.08[a]	0.51 (0.61)[d]
	10	900	0.41 ± 0.09[a]	0.40 (0.49)[d]
$C_6H_5O•$ (**3**) + H•	4	700	0.18 ± 0.08[a]	0.18
	4	800	0.24 ± 0.10[a]	0.21
	4	900	0.33 ± 0.13[a]	0.23
	10	800	0.19 ± 0.09[a]	0.21
	10	900	0.28 ± 0.12[a]	0.23
C_5H_6 (**11**) + CO	4	700	0.22 ± 0.05[a]	0.17
	4	800	0.27 ± 0.06[a]	0.29
	4	900	0.33 ± 0.08[a]	0.40
	10	800	0.21 ± 0.05[a]	0.18
	10	900	0.27 ± 0.07[a]	0.28
$C_5H_5•$ + H• + CO	4	700	0.02 ± 0.01[a]	*b*
or + HCO•	4	800	0.02 ± 0.01[a]	*b*
	4	900	0.02 ± 0.01[a]	*b*
	10	800	0.01 ± 0.01[a]	*b*
	10	900	0.03 ± 0.02[a]	*b*
C_6H_5OH and ($C_6H_5O•$ + H•)	4	300	1.0[c]	0.94 (1.0)[d]
	4	500	1.0[c]	0.84 (1.0)[d]
	4	800	0.78 ± 0.13[c]	0.63 (0.71)[d]
	4	900	0.68 ± 0.15[c]	0.53 (0.60)[d]
	4	1000	0.54 ± 0.15[c]	0.42 (0.49)[d]
	1	800	0.60 ± 0.13[c]	0.45 (0.51)[d]
	10	800	0.84 ± 0.20[c]	0.72 (0.82)[d]
C_5H_6 + CO and	4	300	0.0	0.00
($C_5H_5•$ + H• + CO or HCO•)	4	500	0.0	0.05
	4	800	0.22 ± 0.07[c]	0.29
	4	900	0.34 ± 0.09[c]	0.40
	4	1000	0.43 ± 0.09[c]	0.51
	1	800	0.40 ± 0.13[c]	0.49
	10	800	0.16 ± 0.03[c]	0.18

[a] Time-of-flight mass spectrometer. The 2-σ standard deviations are estimated from uncertainties in the relative cross sections: ±50% for free radicals and ±20% for stable molecules. [b] C_5H_5 radical is excluded from master equation modeling (see text), [c] Magnetic sector mass spectrometer. The 2-σ standard deviations are estimated from uncertainties in the relative cross sections. [d] Values in parentheses include the contributions from other C_6H_6O isomers, including benzene oxide, 2,4-hexadienone and 2,5-hexadienone.

Table 7. Monte Carlo RRKM/master equation results fitted to modified Arrhenius expressions.[a]

		$k(T) = A\,T^n\,e^{-B/T}$			
Reaction channel	P (bar)	A	n	B	T (K)
$C_6H_6 + O(^3P) \rightarrow C_6H_5O\bullet$ (**3**) + H• (k_{1a})	0.1 – 10	3.3×10^{-17}	1.80	2000	500–2000
	50	5.9×10^{-14}	0.91	3182	500–2000
	500	2.2×10^{-12}	0.47	4245	500–2000
$C_6H_6 + O(^3P) \rightarrow C_6H_5OH$ (**9**) (k_{1b})	0.1	2.5×10^{5}	–4.72	6715	500–2000
	1	1.2×10^{-1}	–2.56	7546	500–2000
	10	5.9×10^{0}	–2.82	11024	700–2000
	50	9.7×10^{11}	–5.89	17380	900–2000
	500	7.0×10^{7}	–4.73	19340	900–2000
$C_6H_6 + O(^3P) \rightarrow$ cyclopentadiene (**11**) + CO (k_{1c})	0.1	1.2×10^{-10}	0.12	5927	500–2000
	1	1.0×10^{-8}	–0.49	7546	500–2000
	10	2.3×10^{14}	–6.71	17429	700–2000
	50	2.6×10^{7}	–4.73	16894	700–2000
	500	3.7×10^{32}	–11.69	27981	900–2000
$C_6H_6 + O(^3P) \rightarrow$ Benzene oxide (**5**) (k_{1d})	0.1	1.2×10^{36}	–16.06	7197	300–900
	1	3.8×10^{33}	–14.62	7839	300–1300
	10	2.3×10^{19}	–9.65	6708	300–2000
	50	2.8×10^{14}	–7.79	6799	300–2000
	500	1.9×10^{20}	–9.06	10546	300–2000
$C_6H_6 + O(^3P) \rightarrow$ 2,4–cyclohexadienone (**7**) (k_{1e})	0.1	3.8×10^{4}	–4.97	4785	500–2000
	1	2.0×10^{1}	–3.72	5001	500–2000
	10	4.7×10^{12}	–6.77	9532	500–2000
	50	5.0×10^{4}	–4.20	9265	500–2000
	500	6.9×10^{-14}	1.16	6657	500–2000
$C_6H_6 + O(^3P) \rightarrow$ 2,5–cyclohexadienone (**8**) (k_{1f})	0.1	3.2×10^{3}	–4.71	4785	300–2000
	1	5.7×10^{4}	–4.74	6663	300–2000
	10	1.7×10^{22}	–9.45	14283	500–2000
	50	3.7×10^{17}	–10.50	20429	500–2000
	500	6.1×10^{14}	–6.58	21415	900–2000
$C_6H_6 + O(^3P) \rightarrow [\mathbf{5},\mathbf{7},\mathbf{8}]_{ss} \rightarrow C_6H_5OH$ (**9**) ($k_{1c\text{-}def}^{eff}$)[b]	0.1	9.3×10^{1}	–4.19	3886	500–2000
	1	2.5×10^{-3}	–2.60	3364	500–2000
	10	8.9×10^{-10}	–0.60	2001	500–2000
	50	1.2×10^{-8}	–0.84	2628	500–2000
	500	1.5×10^{-2}	–2.40	5571	700–2000
$C_6H_6 + O(^3P) \rightarrow [\mathbf{5},\mathbf{7},\mathbf{8}]_{ss} \rightarrow C_5H_6$ (**11**) + CO ($k_{1c\text{-}def}^{eff}$)[b]	0.1	3.8×10^{12}	–7.09	11793	500–2000
	1	1.2×10^{5}	–4.66	10469	500–2000
	10	2.5×10^{6}	–4.90	11211	700–2000
	50	5.2×10^{-1}	–2.88	9730	500–2000
	500	1.6×10^{-12}	0.56	6913	900–2000

[a] Units are $cm^3molecule^{-1}s^{-1}$ and K. Rates computed with helium as the bath gas. [b] Pseudo-steady state rate expressions derived from expressions of k_{1d}, k_{1e}, k_{1f}, and the high-pressure limit rate constants for benzene oxide, 2,4-cyclohexadienone and 2,5-cyclohexadienone isomerization to form phenol and dissociation to cyclopentadiene and CO (see text).

Figure Captions

Figure 1. Arrhenius plot for of the total rate constant of reaction R1. ◢: ref 14 (28 Bar in Ar); ×: ref 15 (50-110 Torr in He); ●: ref 16 (30-90 Torr in N_2O); ■: ref 17 (30-90 Torr in N_2O); ◇: ref 18 (40-80 Torr in N_2O); △: ref 19 (26 Torr in Ar); □: ref 20 (100 Torr in Ar); ▲: ref 22 (2 Torr in Ar); +: ref 23 (270-850 Torr in He); ○: ref 24 (180-450 Torr Ar).

Figure 2. Time-resolved mass spectrum observed at 900 K and 4 Torr for reaction R1, integrated over photon energies from 7.9 eV to 9.1 eV.

Figure 3. Photon energy resolved mass spectrum observed at 900 K and 4 Torr for reaction R1, integrated over the first 20 ms following the photolysis pulse.

Figure 4. Relative integrated mass signals, taken at 9.1 eV photon energy, determined for the products of reaction R1 with m/z = 65-66 (top panel) and 93-94 (bottom panel) at 900 K and 10 Torr.

Figure 5. Potential energy surfaces of reaction R1.

Figure 6. Geometry parameters determined at the EOM-EE-CCSD/6-311G(2d,p) level of theory. Bond lengths are in Angstroms.

Figure 7. Frontier MOs of the C_6H_6O adduct at the $^3A'$ state geometry computed with the 6-311G(2d,p) basis. In the open-shell diradical state, the a′ π*-like orbital is always singly occupied, whereas different populations of the a″ or a′ lone pair orbitals give rise to the A′ and A″ electronic states, respectively. Note that the singlet states are of open-shell character.

Figure 8. Photoionization efficiency of the observed m/z = 94 product of the O + benzene reaction for phenol at 900 K (symbols), compared to the calibration spectrum of phenol (line).

Figure 9. Branching ratios observed as a function of temperature at 4 Torr for (a) m/z=94/93 and m/z=66/65 by magnetic sector mass spectrometer (filled symbols) and time-of-flight mass spectrometer (open symbols), and (b) branching ratios determined by time-of-flight mass spectrometer. Lines are drawn to guide the eye.

Figure 10. Branching ratios observed as a function of pressure at 800 K for (a) m/z=94/93 and m/z=66/65 by magnetic sector mass spectrometer (filled symbols) and time-of-flight mass spectrometer (open symbols), and (b) branching ratios determined by time-of-flight mass spectrometer. Lines are drawn to guide the eye.

Figure 11. Branching fractions calculated for reaction channels (a) phenol, (b) phenoxy + H, (c) cyclopentadiene + CO, (d) benzene oxide, (e) 2,4-cyclohexadienone, and (f) 2,5-cyclohexadienone (helium bath gas). The branching ratio of the initial adduct is excluded from the above plot (see text).

Figure 12. Arrhenius plots for the reaction channels leading to (a) phenol, (b) phenoxy + H, (c) cyclopentadiene + CO, (d) benzene oxide, (e) 2,4-cyclohexadienone, and (f) 2,5-cyclohexadienone. Symbols are rates computed with Monte Carlo RRKM/master equation modeling and lines represent fitted Arrhenius expressions (Table 7).

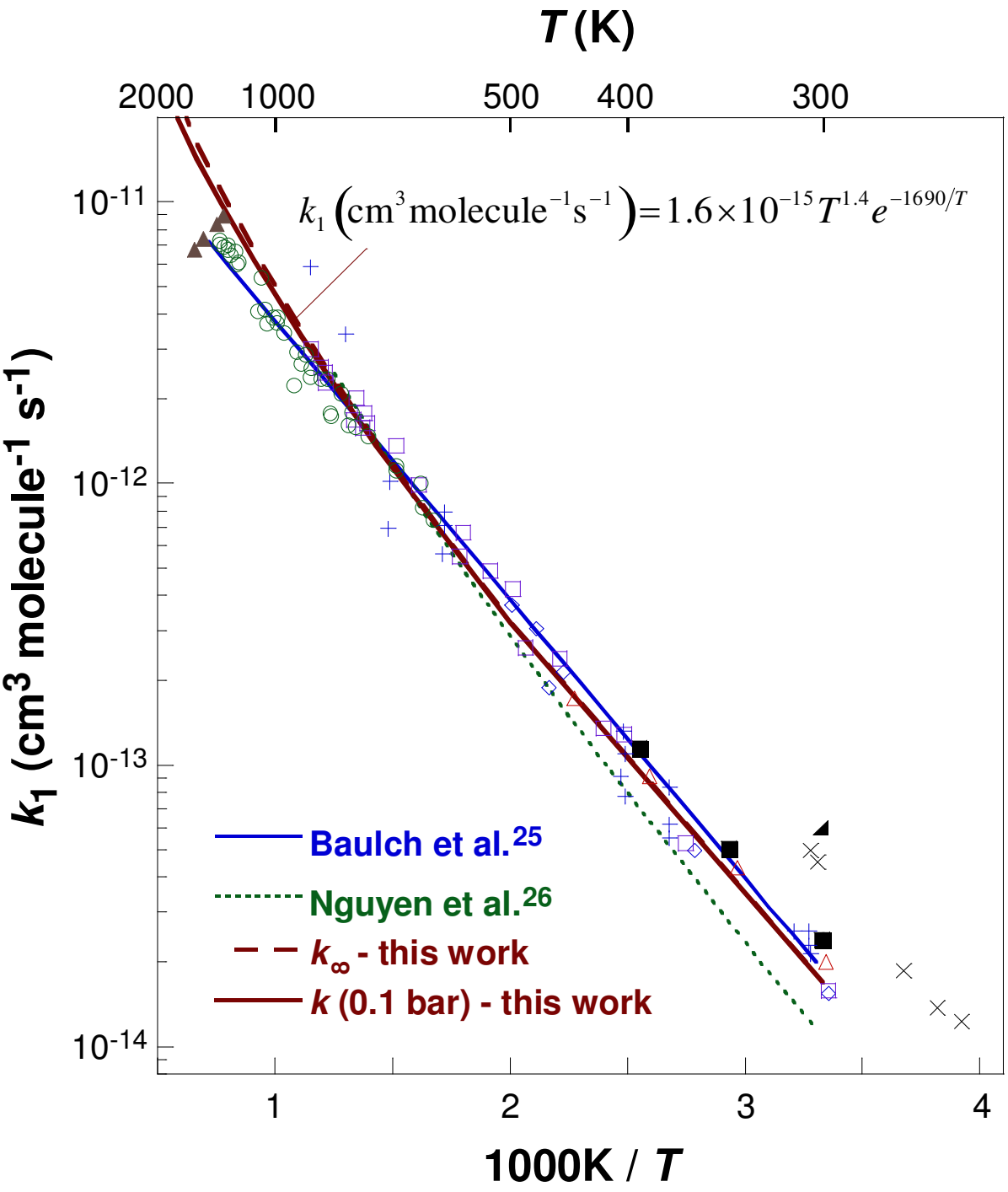

Figure 1. Arrhenius plot for the total rate constant of reaction R1. ◢: ref 14 (28 Bar in Ar); ×: ref 15 (50-110 Torr in He); ●: ref 16 (30-90 Torr in N_2O); ■: ref 17 (30-90 Torr in N_2O); ◇: ref 18 (40-80 Torr in N_2O); △: ref 19 (26 Torr in Ar); □: ref 20 (100 Torr in Ar); ▲: ref 22 (2 Torr in Ar); +: ref 23 (270-850 Torr in He); ○: ref 24 (180-450 Torr Ar).

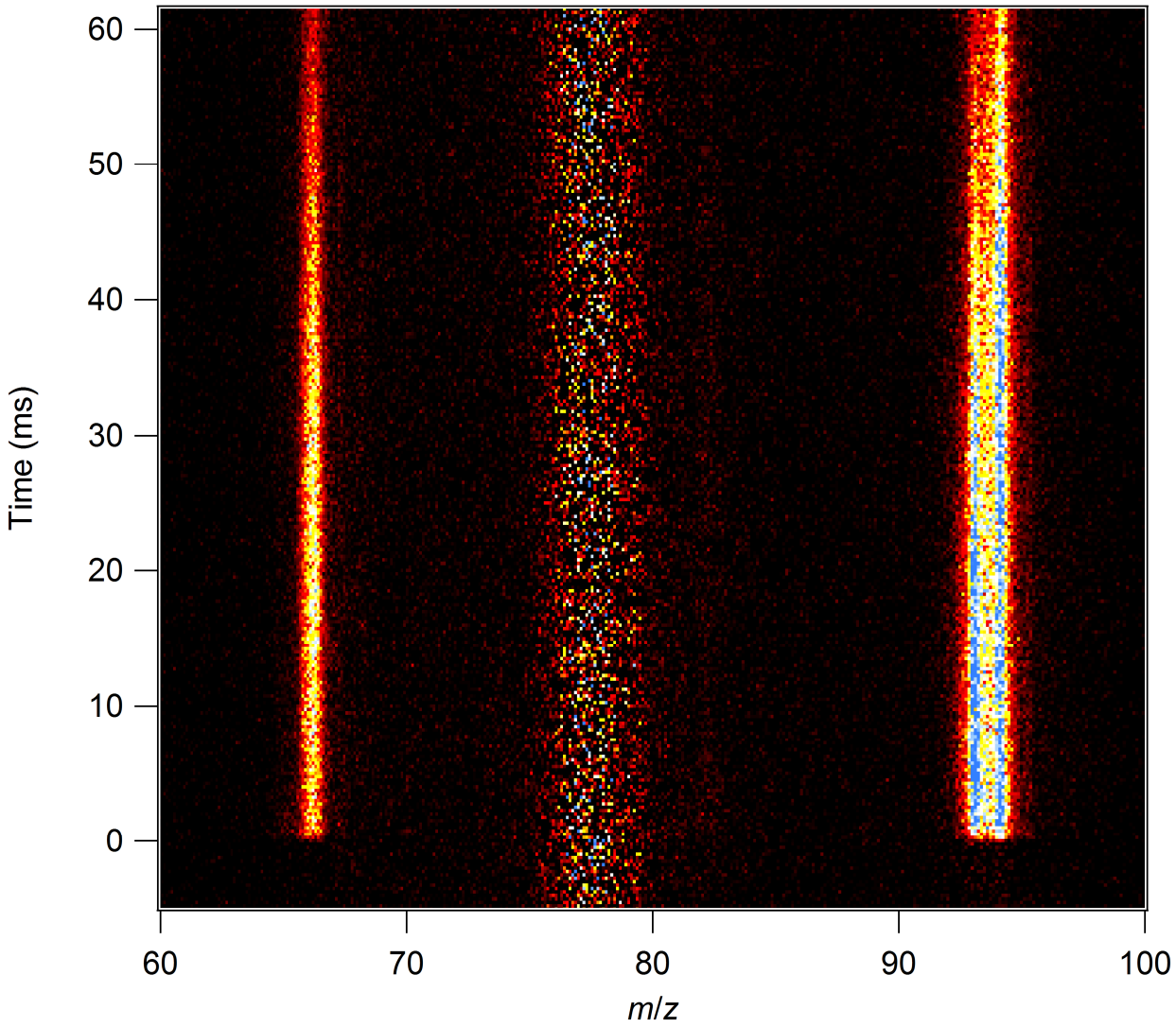

Figure 2. Time-resolved mass spectrum observed at 900 K and 4 Torr for reaction R1, integrated over photon energies from 7.9 eV to 9.1 eV.

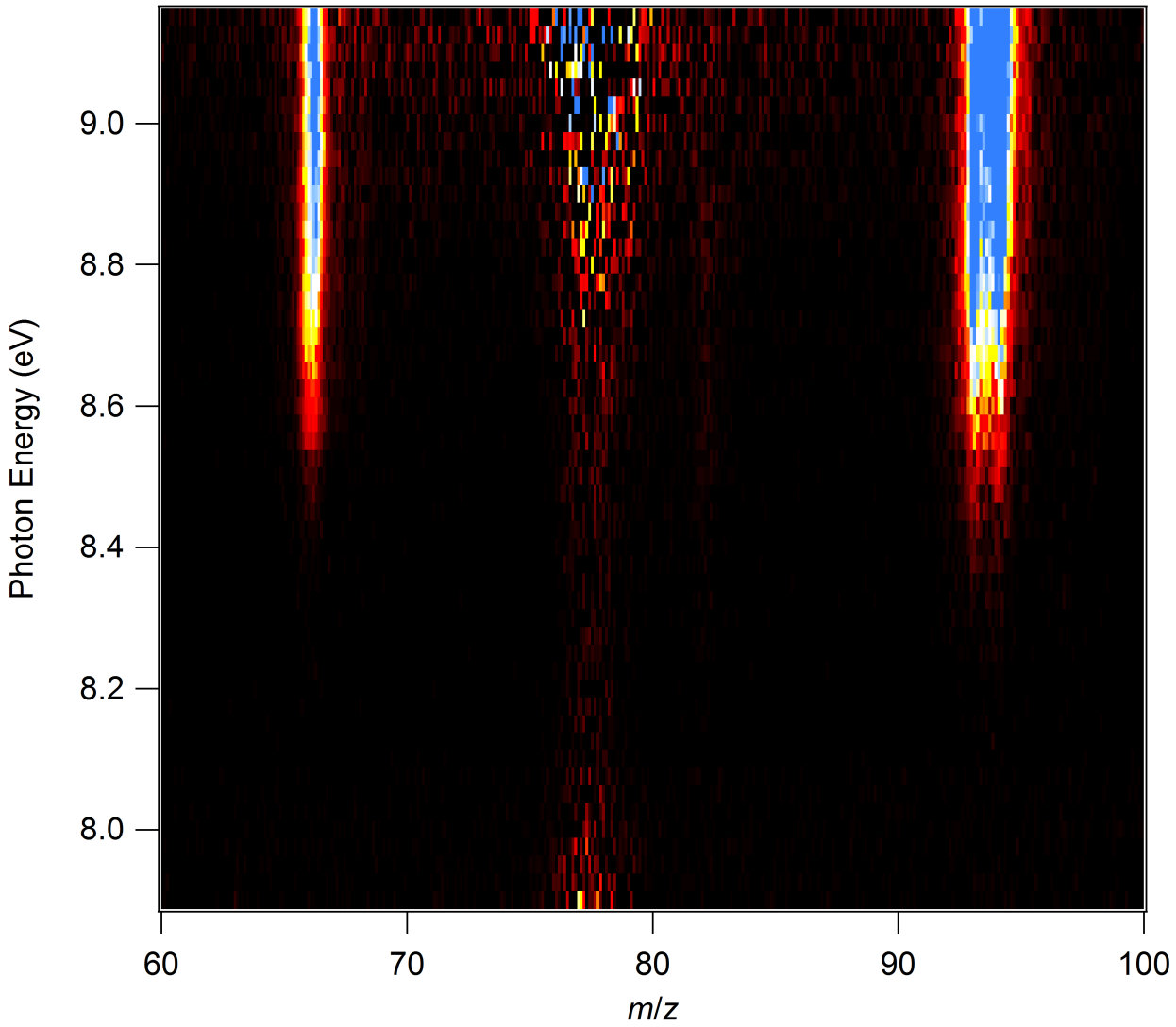

Figure 3. Photon energy resolved mass spectrum observed at 900 K and 4 Torr for reaction R1, integrated over the first 20 ms following the photolysis pulse.

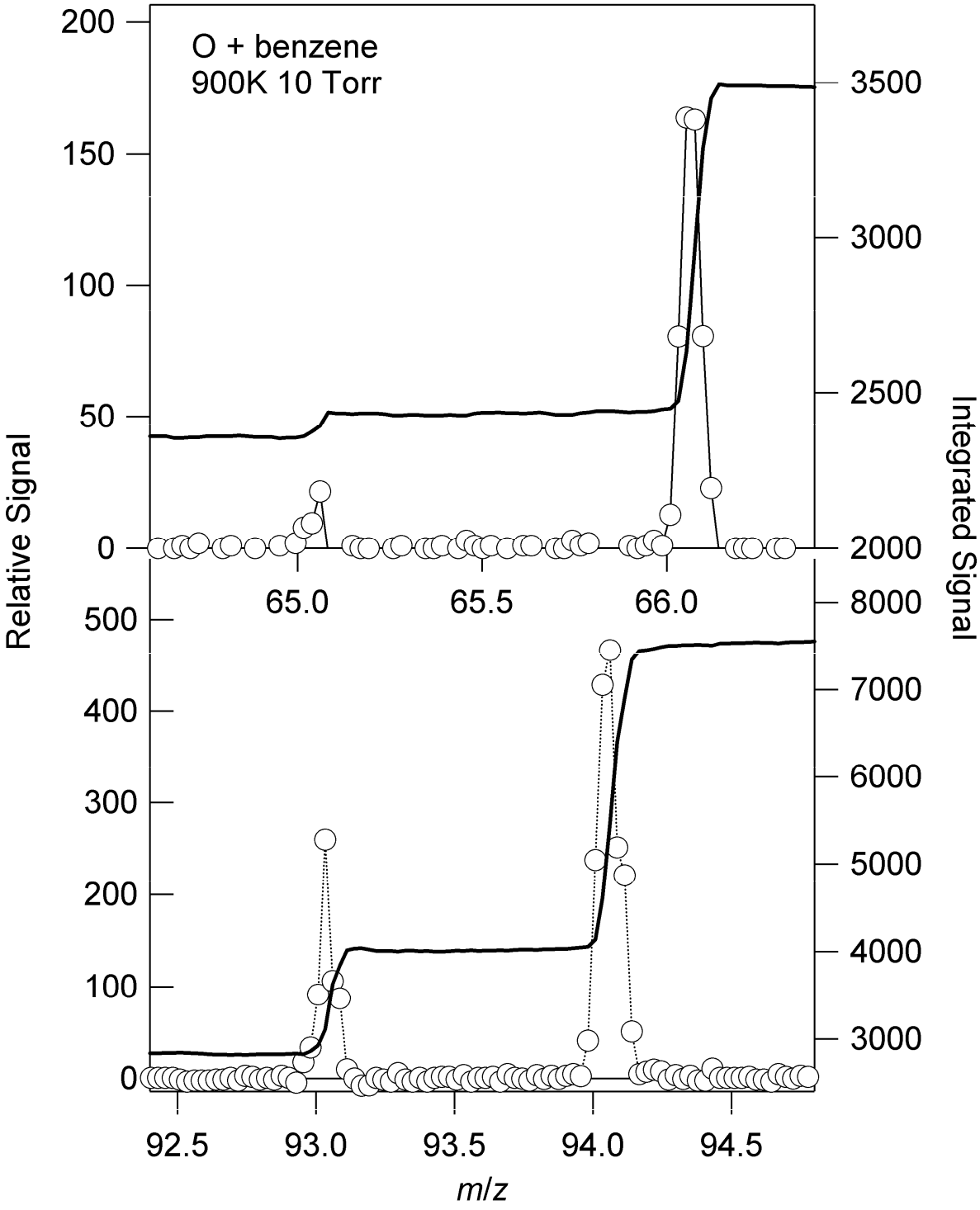

Figure 4. Relative integrated mass signals, taken at 9.1 eV photon energy, determined for the products of reaction R1 with m/z = 65-66 (top panel) and 93-94 (bottom panel) at 900 K and 10 Torr.

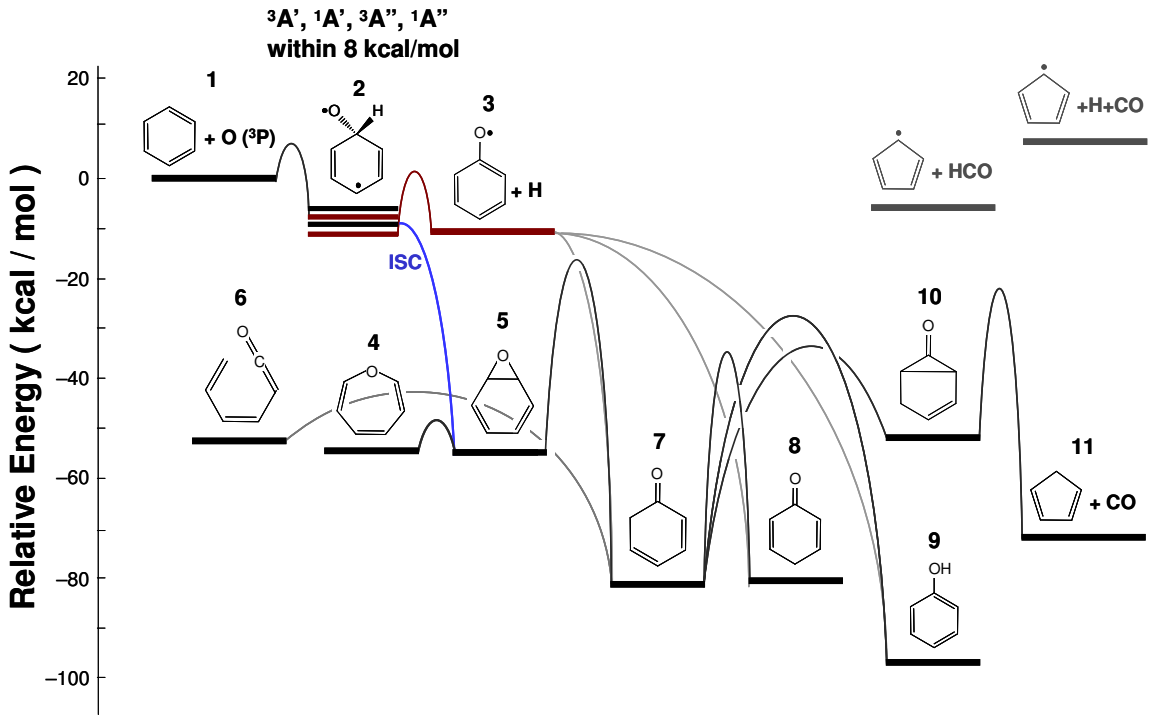

Figure 5. Potential energy surfaces of reaction R1.

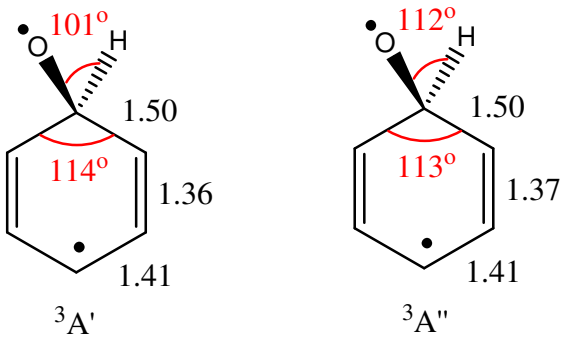

Figure 6. Geometry parameters determined at the EOM-EE-CCSD/6-311G(2d,p) level of theory. Bond lengths are in Angstroms.

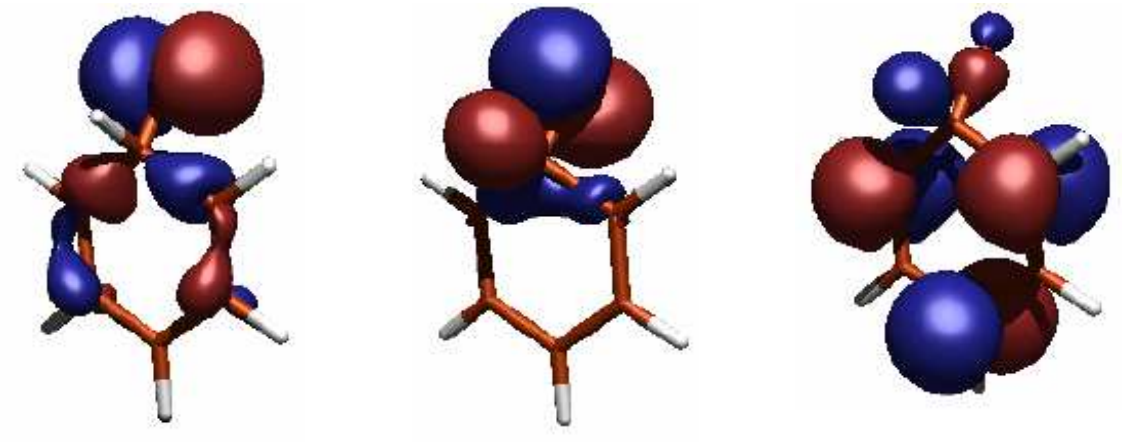

a″ lone pair (n_{oop}) a′ lone pair (n_{ip}) a′ (π^*)

Figure 7. Frontier MOs of the C_6H_6O adduct at the $^3A'$ state geometry computed with the 6-311G(2d,p) basis. In the open-shell diradical state, the a′ π^*-like orbital is always singly occupied, whereas different populations of the a″ or a′ lone pair orbitals give rise to the A′ and A″ electronic states, respectively. Note that the singlet states are of open-shell character.

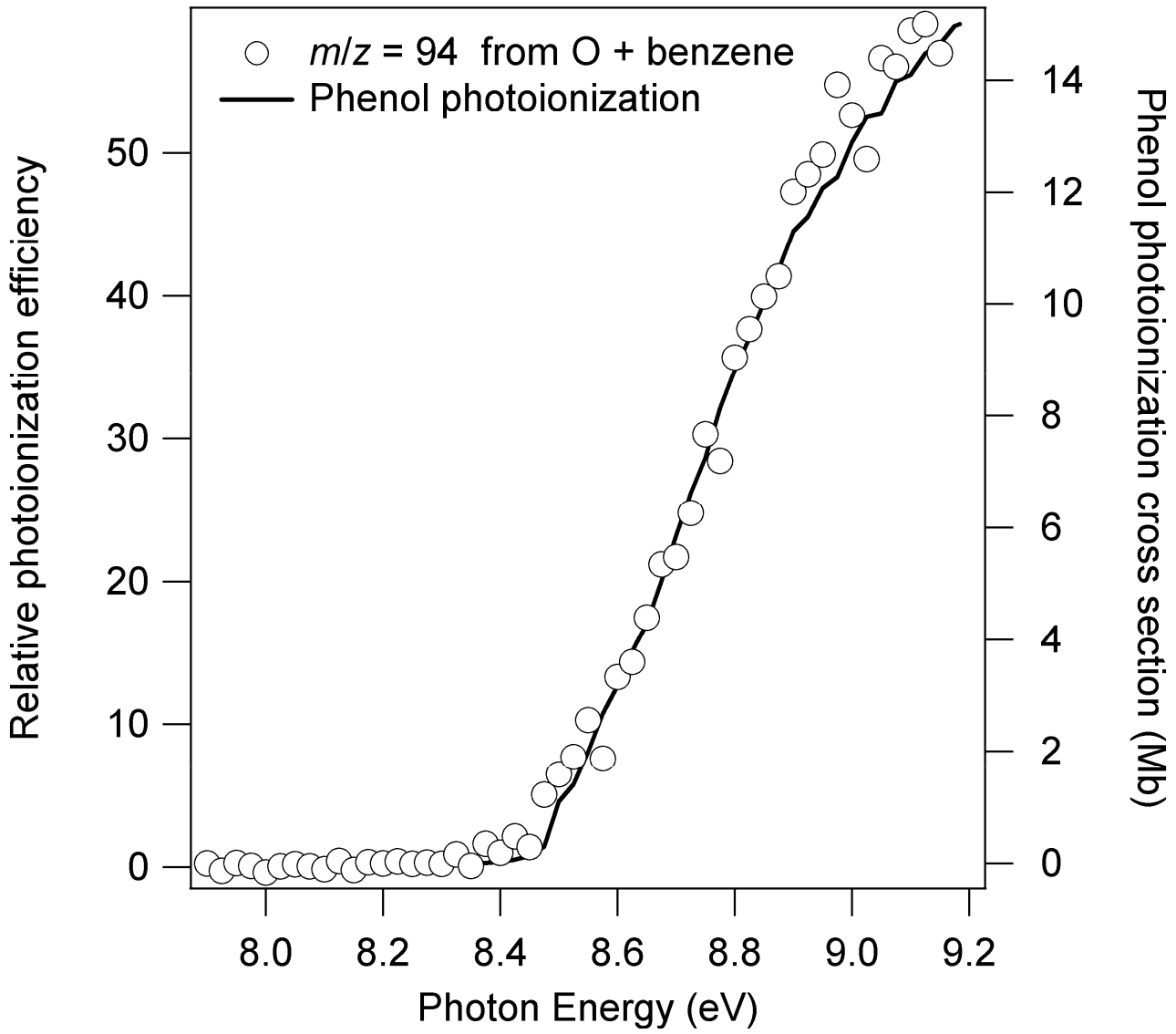

Figure 8. Photoionization efficiency of the observed m/z = 94 product of the O + benzene reaction for phenol at 900 K (symbols), compared to the calibration spectrum of phenol (line).

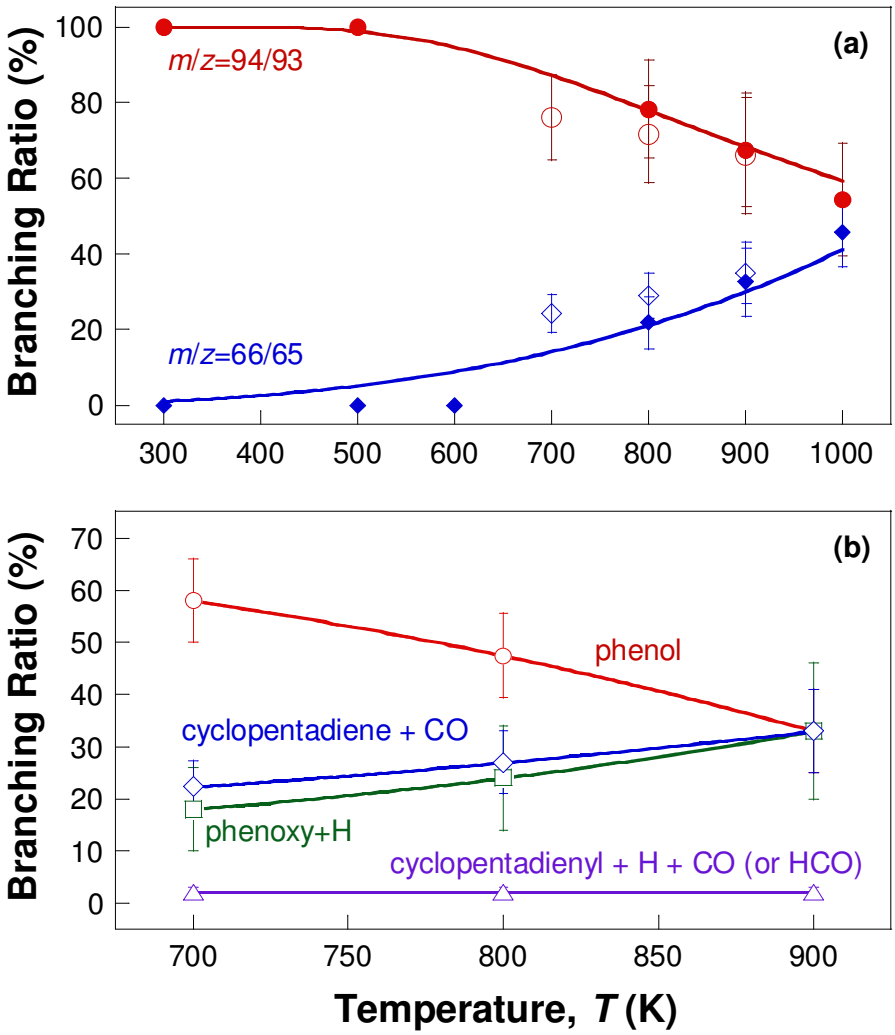

Figure 9. Branching ratios observed as a function of temperature at 4 Torr for (a) *m*/*z*=94/93 and *m*/*z*=66/65 by magnetic sector mass spectrometer (filled symbols) and time-of-flight mass spectrometer (open symbols), and (b) branching ratios determined by time-of-flight mass spectrometer. Lines are drawn to guide the eye. Error bars represent 2σ-standard deviations.

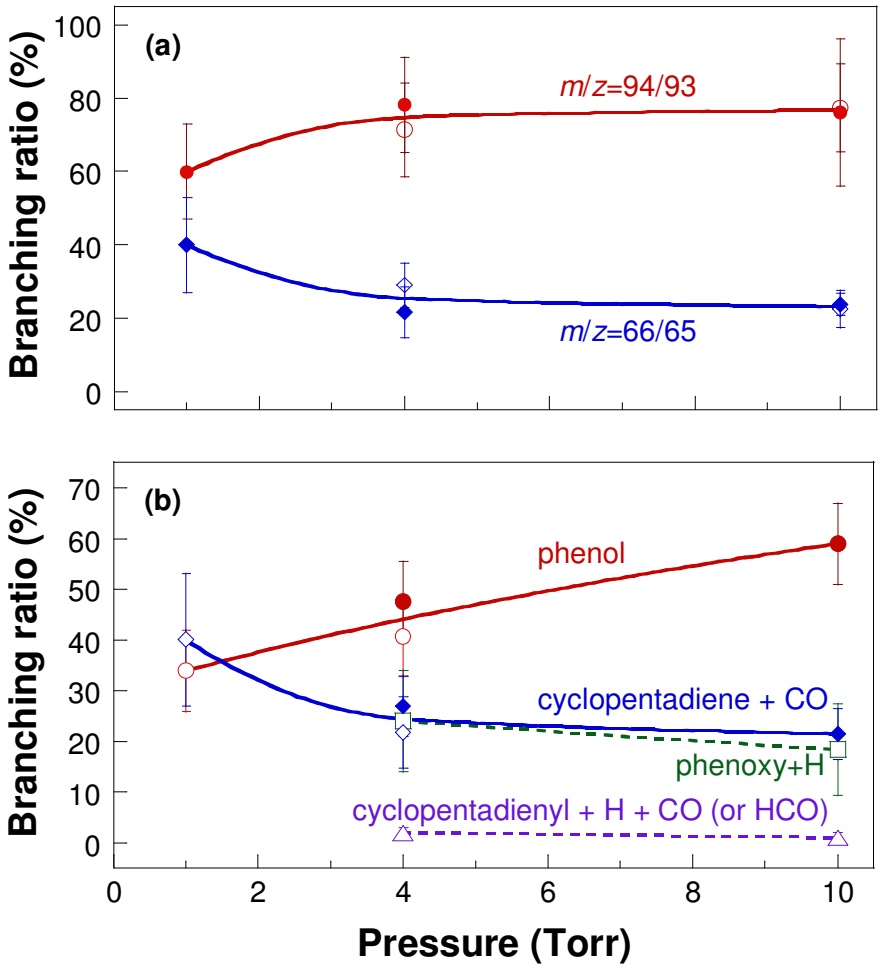

Figure 10. Branching ratios observed as a function of pressure at 800 K for (a) *m*/*z*=94/93 and *m*/*z*=66/65 by magnetic sector mass spectrometer (filled symbols) and time-of-flight mass spectrometer (open symbols), and (b) branching ratios determined by time-of-flight mass spectrometer. Lines are drawn to guide the eye. Error bars represent 2-σ standard deviations.

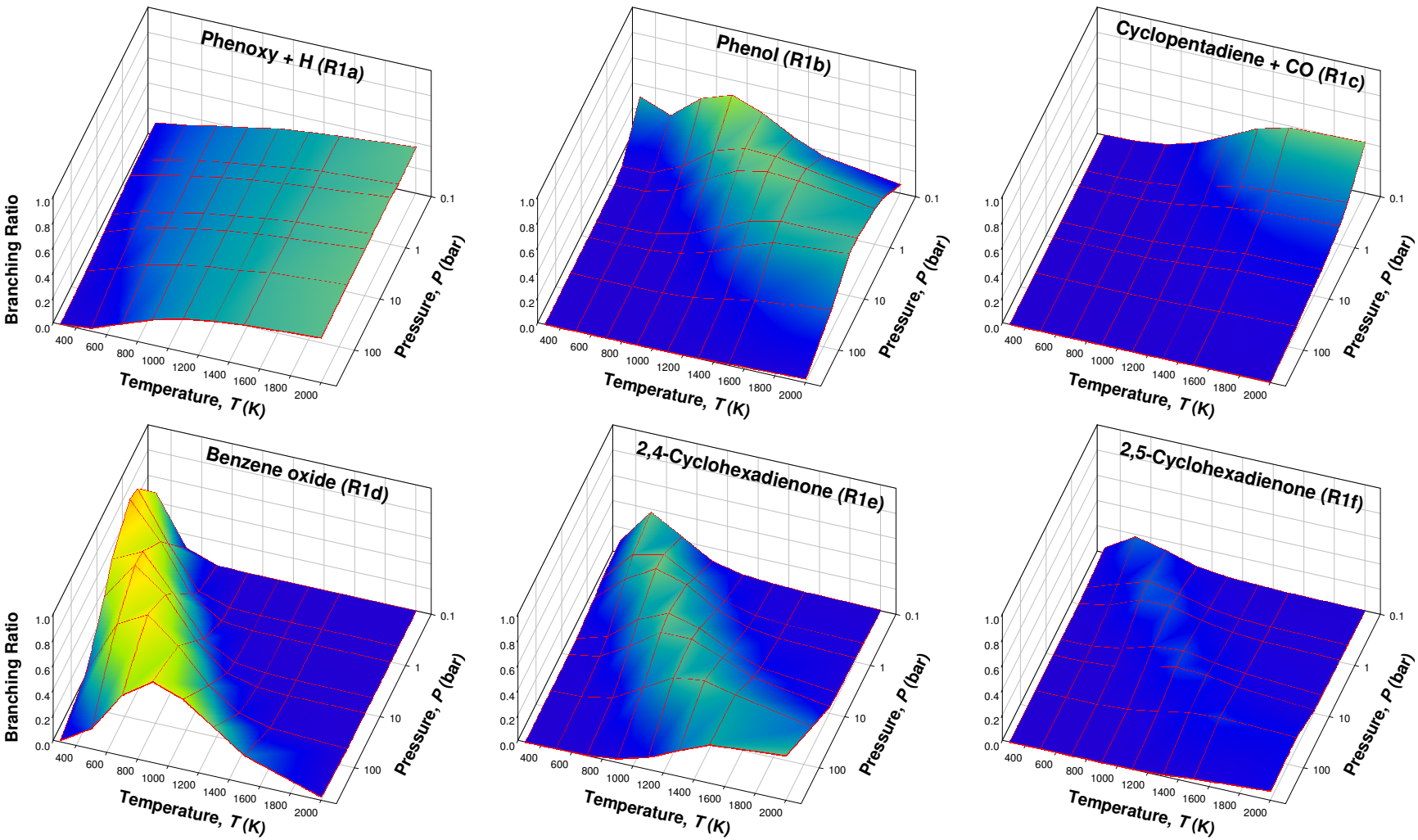

Figure 11. Branching fractions calculated for reaction channels (a) phenol, (b) phenoxy + H, (c) cyclopentadiene + CO, (d) benzene oxide, (e) 2,4-cyclohexadienone, and (f) 2,5-cyclohexadienone (helium bath gas). The branching ratio of the initial adduct is excluded from the above plot (see text).

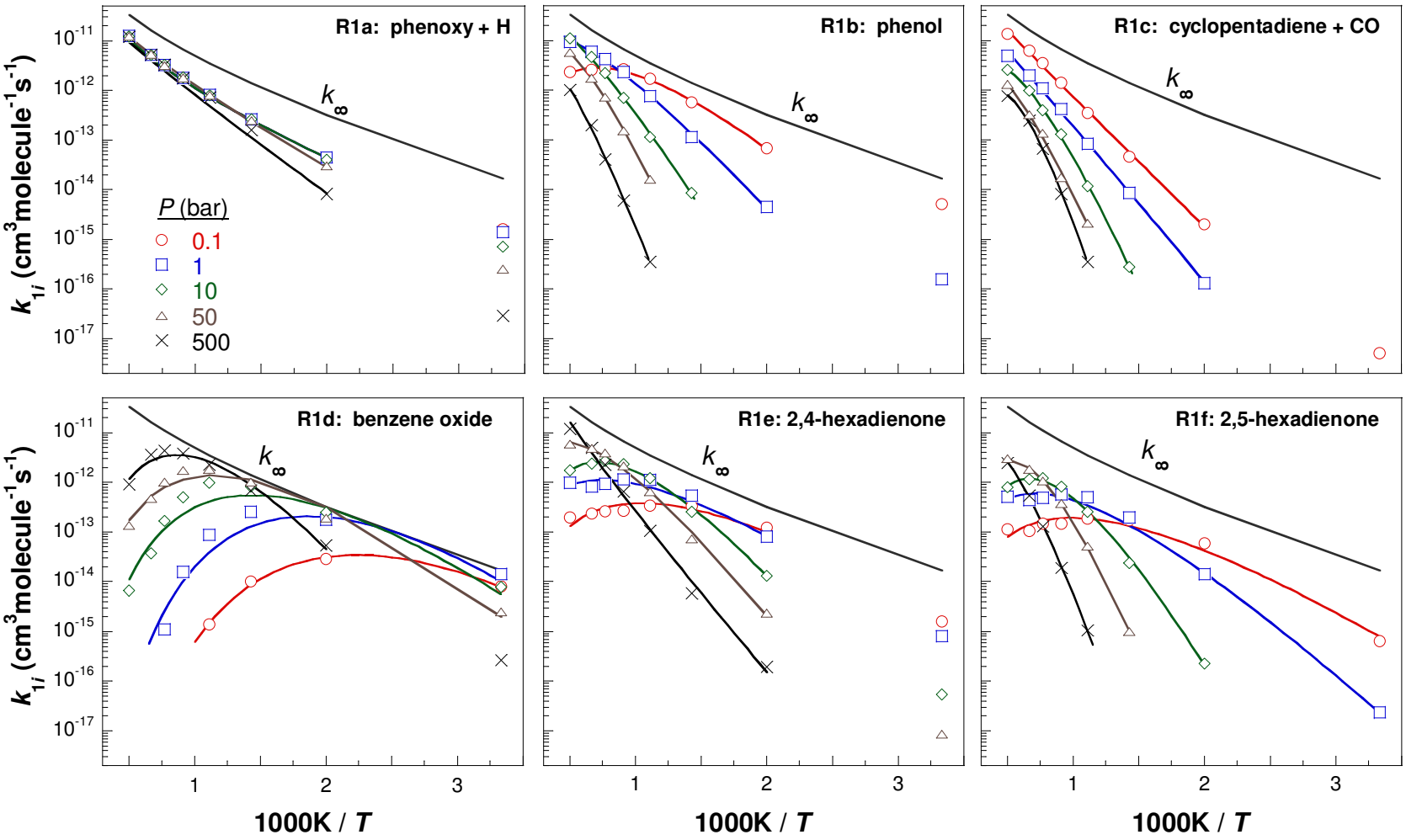

Figure 12. Arrhenius plots for the reaction channels leading to (a) phenol, (b) phenoxy + H, (c) cyclopentadiene + CO, (d) benzene oxide, (e) 2,4-cyclohexadienone, and (f) 2,5-cyclohexadienone. Symbols are rates computed with Monte Carlo RRKM/master equation modeling and lines represent fitted Arrhenius expressions (Table 7).